

ION BEAMS PROVIDED BY SMALL ACCELERATORS FOR MATERIAL SYNTHESIS AND CHARACTERIZATION

A. Mackova^{a,b}

*^aNuclear Physics Institute of the Academy of Sciences of the Czech Republic v.
v. i., 250 68 Rez, Czech Republic*

*^bDepartment of Physics, Faculty of Science, J.E. Purkinje University, Ceske
mladeze 8, 400 96 Usti nad Labem, Czech Republic*

mackova@ujf.cas.cz

<http://neutron.ujf.cas.cz/en/instruments/tandetron>



EUROPEAN UNION
European Structural and Investment Funds
Operational Programme Research,
Development and Education



CONTENTS

- **INTRODUCTION**
 - **ION BEAMS APPLICATION ON ELEMENTAL ANALYSIS AND ION BEAM MODIFICATION**
- **EXPERIMENTAL**
 - **ACCELERATOR TANDETRON**
 - **MAIN PRINCIPLES OF ION BEAM ANALYTICAL METHODS**
 - **ION BEAM IMPLANTATION AND ION MICROBEAM**
- **RESULTS**
 - **ION BEAM ANALYSIS FOR OPTICS AND SPINTRONICS**
 - **NANOSTRUCTURE SYNTHESIS USING ION BEAM IMPLANTATION**
 - **MATERIAL RESEARCH APPLICATION**
- **CONCLUSIONS**

INTRODUCTION

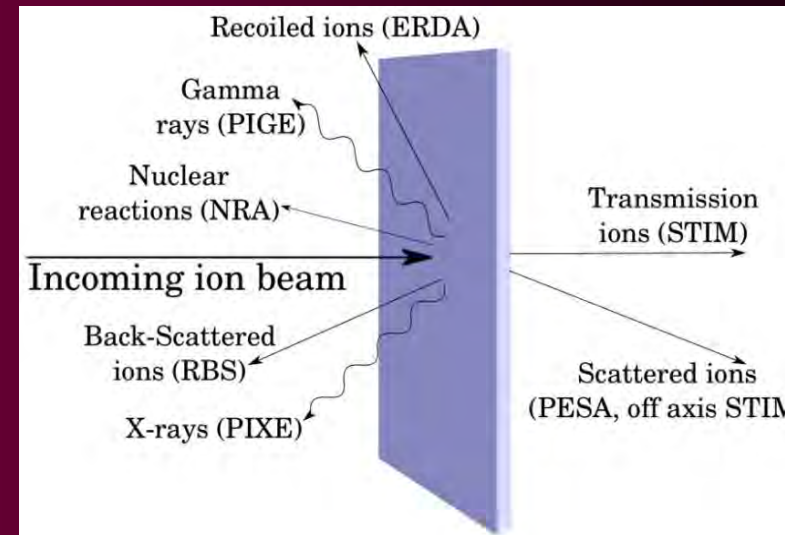
As a result of ion beam irradiation of a material, two types of collision occur: inelastic collisions and elastic collisions.

In inelastic collisions two phases exist. In the first phase particles are emitted (NRA – Nuclear Reaction Analysis). This is followed in the second phase by the emission of γ -rays (PIGE – Particle Induced Gamma-ray Emission spectroscopy) or X-rays (PIXE – Particle Induced X-ray Emission spectroscopy).

In elastic collisions two main phenomena are taking place: (i) the primary ion beam is back-scattered and is used in Rutherford Back-Scattering spectrometry (RBS) and (ii) lighter atomic nuclei can be ejected, recoiling from the heavier projectile ions. This is the principle of Elastic Recoil Detection Analysis (ERDA).

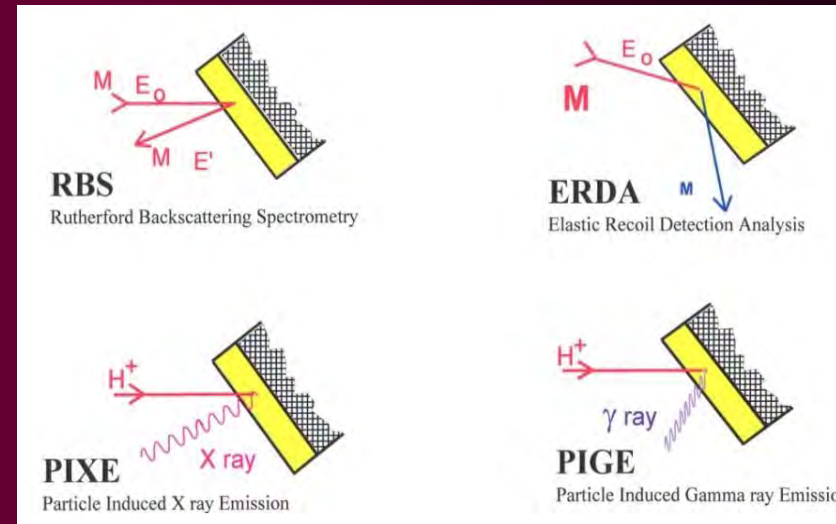
The IBA methods employ ion beams of various elements with kinetic energy ranging from hundreds of keV up to tens of MeV, beam currents are at most units of microA. For production of the probing ions different types of mostly electrostatic accelerators (single-ended Van de Graaf or Cockroft-Walton accelerator, Tandatron) are utilised.

The information about investigated samples is provided via measurement of energy spectra of scattered ions, recoiled atoms or secondary radiation induced by ion bombardment.



INTRODUCTION

- Modification of crystalline materials and glasses by ion implantation, preparation of nano-structures with significant optical, magnetic or electrical properties.
- Ion beam analysis of multi-layered, crystalline, amorphous materials for optics, electronics, spintronics.
- MC modelling of ion and matter interaction, defect creation, radiation damage, ion beam transfer through crystalline samples.
- 3D elemental mapping using ion microprobe it means the focused ion beam irradiation.
- Trace elements study in aerosols for the environmental studies.
- Ion beam micromachining, optical microstructure deposition.
- Study of energetic ion interaction with matter, energy losses and energy straggling, fundamental study of ion interaction with solids.
- Irradiation of the living cells using external beam of energetic ions for dosimetry.
- Study of chemical composition of the materials for nuclear power plants (nuclear fuel rods, study of heavy element diffusion in rocks for nuclear waste storage), materials for nuclear fusion.
- Characterization of materials for biomedicine, environmental research, archaeometry.



ACCELERATOR TANDETRON

RBS (Rutherford Back-Scattering spectrometry)
ERDA (Elastic Recoil Detection Analysis)
PESA (Proton Elastic Scattering Analysis)
PIXE (Particle Induced X-ray Spectroscopy)
PIGE (Particle Induced Gamma-Ray Spectroscopy)
NRA (Nuclear Reaction Analysis)
TOF-ERDA (Time of Flight ERDA)
RBS-channeling
Ion implantation

Ion energy E, terminal voltage U_T

$$E = (n+1) \cdot U_T$$

Tandetrion 4130 MC, Nuclear Physics Institute, Prague

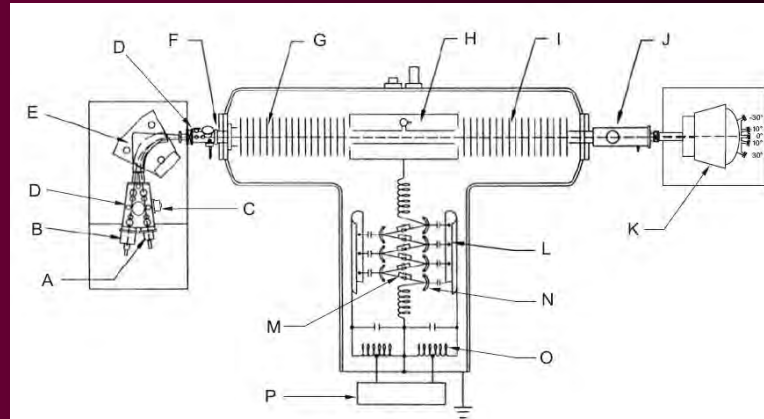
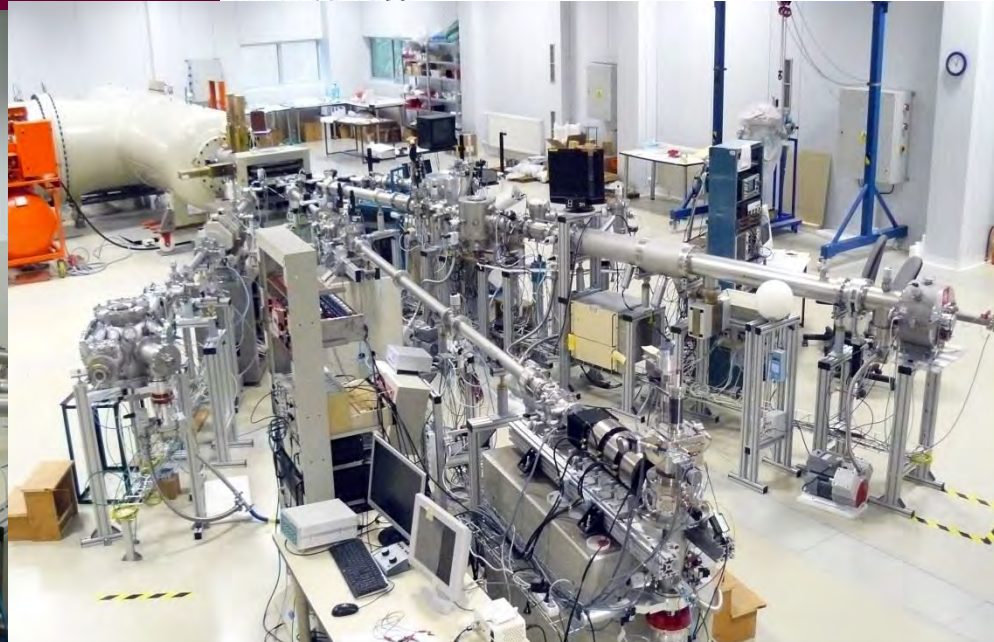


Figure 2.2: The scheme of the Tandetrion 4130 MC. Labelled parts: Duoplasmatron ion source (A), Cs sputter ion source (B), Li charge exchange canal (C), Ion optics elements (D), 90° switching/analyzing magnet (E), Q-snout lens (F), Low-energy accelerator tube (G), HV terminal with gas stripper (H), High-energy accelerator tube (I), Electrostatic quadrupole triplet lens (J), High-energy switching/analyzing magnet (K), Rf driver electrode (L), Rectifier stack (M), Capacitor coupling ring (N), Rf oscillator coil (O), Rf driver (P). Ref. [9].



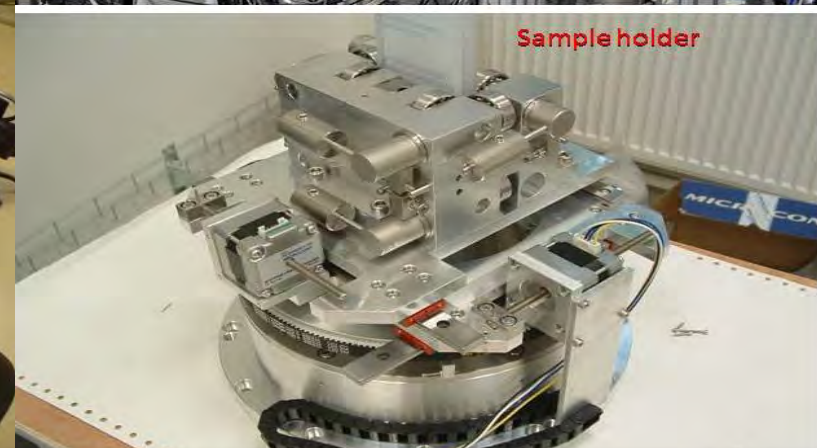
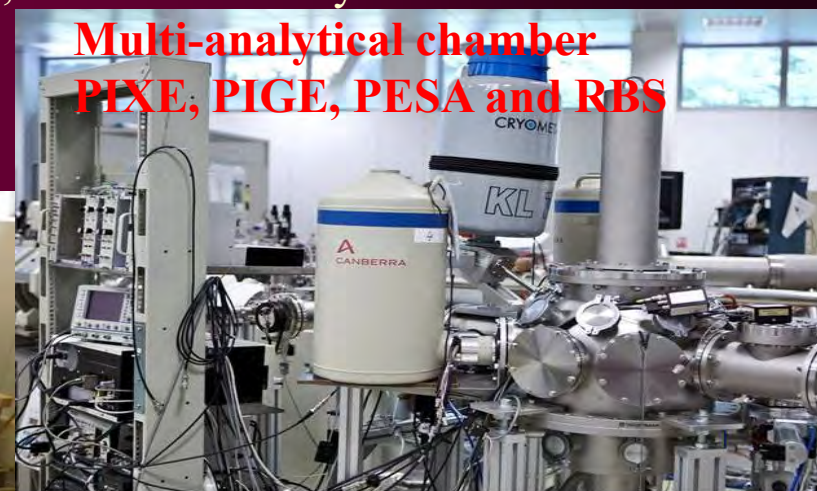
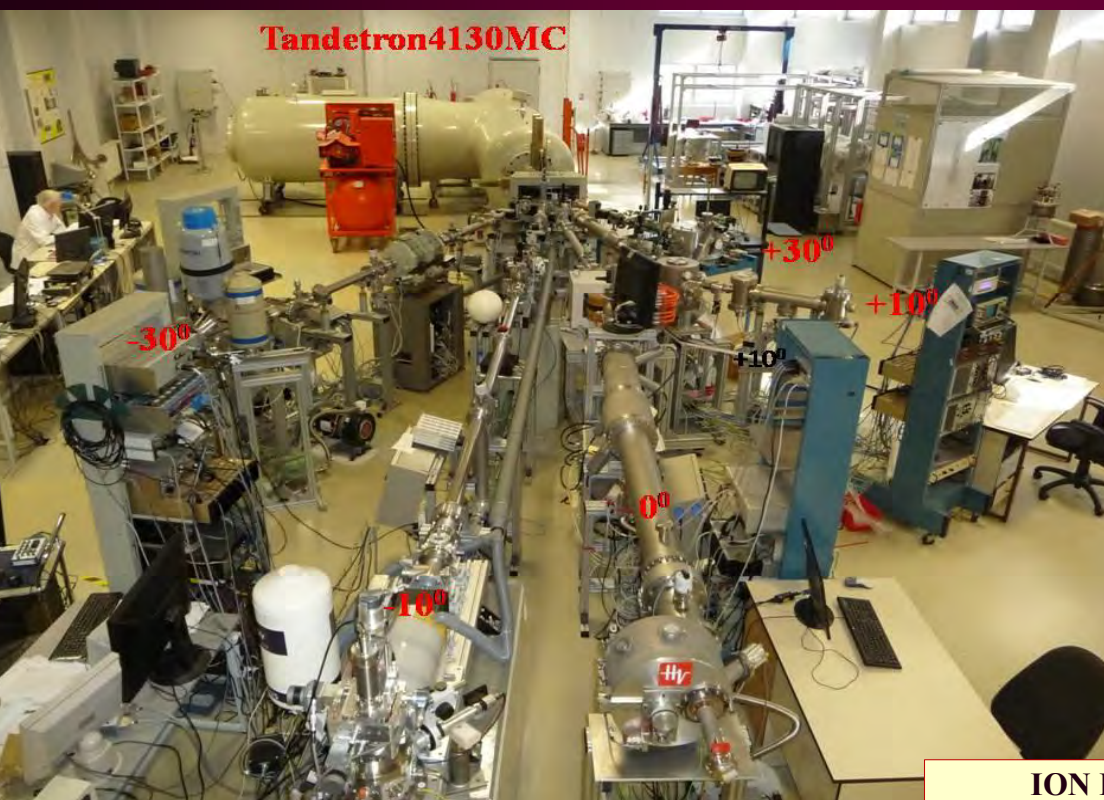
ION BEAMS PROVIDED BY SMALL ACCELERATOR

ION BEAM ANALYTICAL METHODS

Particle Induced X-ray Emission spectroscopy (PIXE),
Particle Induced Gamma-ray Emission spectroscopy (PIGE) and Proton Elastic Scattering
Analysis (PESA)

Ion-Microprobe with 1 μm lateral resolution, external beam accessories for on air irradiation
High-energy ion implantation - modification of materials, nano-structure synthesis.

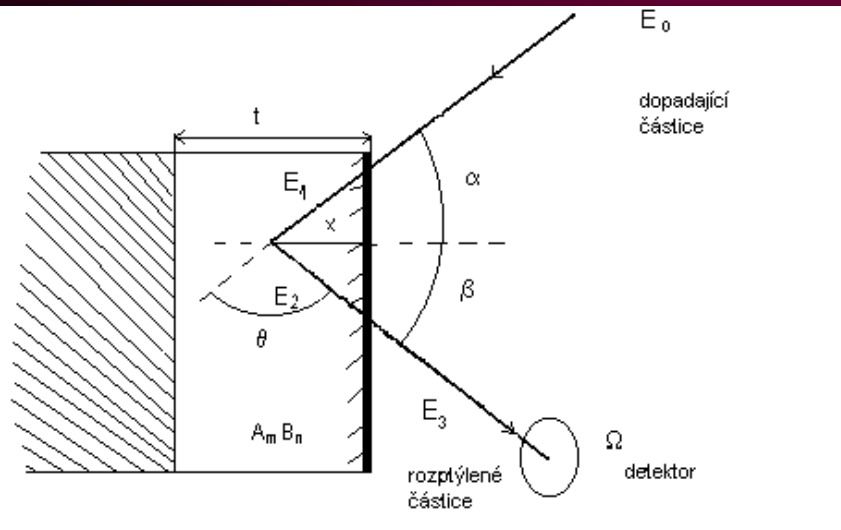
Scanning Ion Microprobe – enables precise lateral
elemental mapping.



ION BEAMS PROVIDED BY SMALL ACCELERATOR

RUTHERFORD BACK-SCATTERING SPECTROMETRY - RBS

RBS (Rutherford Back-scattering Spectrometry) is non-destructive nuclear method for elemental depth analysis of nm-to- μm thick films. It involves measurement of the number and energy distribution of energetic ions (usually MeV light ions such He^+) back-scattered from the atoms within the near-surface region of solid targets.



A projectile ion of the mass M_1 , atomic number Z_1 and initial kinetic energy E_0 penetrates the sample into the depth x , where it elastically scatters from a target atom of the mass M_2 and atomic number Z_2 under the scattering angle θ , having kinetic energy E_2 . The back-scattered ion escapes from the sample with kinetic energy E_3 .

$$E_1 = E_0 - \Delta E_{in}$$

$$E_3 = E_2 - \Delta E_{out}$$

We have to take into account the energetic losses of ions ΔE_{in} penetrating to the depth x and the energetic losses of ions ΔE_{out} after elastic collision. Energy losses are described by linear stopping power S_p , which is a function of energy

$$\Delta E_{in} = S_p(E_0) \cdot \frac{x}{\cos \alpha}$$

$$S_p(E_0) = -\frac{dE}{dx}$$

$$E_2 = K \cdot E_1 = \left(\frac{M_1 \cdot \cos \theta + \sqrt{M_2^2 - M_1^2 \cdot \sin^2 \theta}}{M_1 + M_2} \right)^2 \cdot E_1$$

Number of back-scattered ions in the spectra Q_D is given by the cross section of elastic scattering $\sigma(\theta)$, the detector solid angle Ω , the flux of ions Q and areal density of target N_S .

$$Q_D = \sigma(\theta) \cdot \Omega \cdot Q \cdot N_S$$

RUTHERFORD BACK-SCATTERING SPECTROMETRY - RBS

Detection limit 10^{13} atoms/cm².

Mass resolution should be improved using heavy ion projectiles $\Delta M < 2$

Rutherford differential cross section

$$\frac{d\sigma}{d\Omega} = \frac{(Z_1 Z_2 e^2)^2}{16E^2} \frac{1}{\sin^4 \Theta/2}$$

Measurement of light elements
 - sensitivity will be improved using resonance cross sections
 2,4 MeV H⁺ - C, N, O, Si
 3,04 MeV He⁺ - O

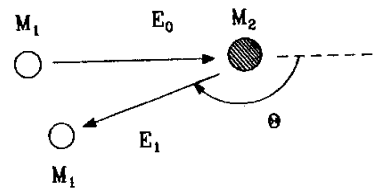


FIGURE 2. Schematics of an elastic collision and backscattering of a lighter projectile of mass M_1 , with a heavier target particle of mass M_2 , initially at rest in the laboratory. The recoil of the target is not plotted.

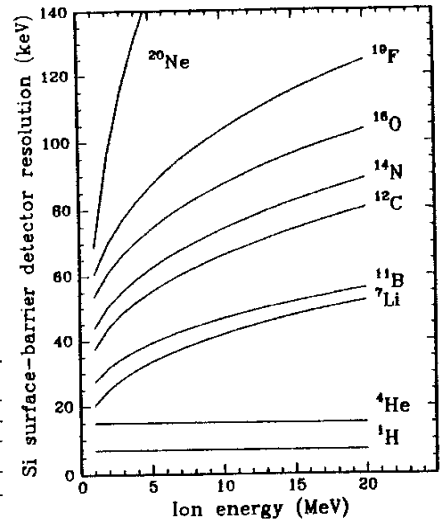
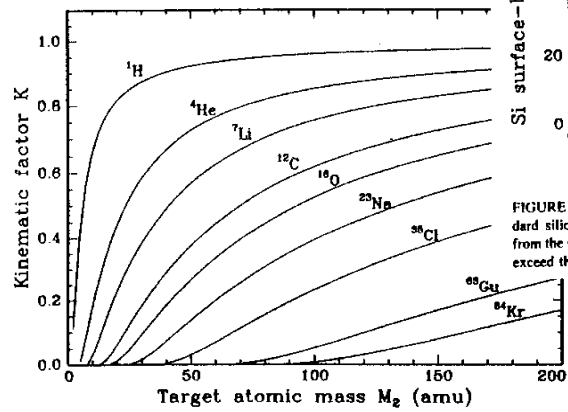
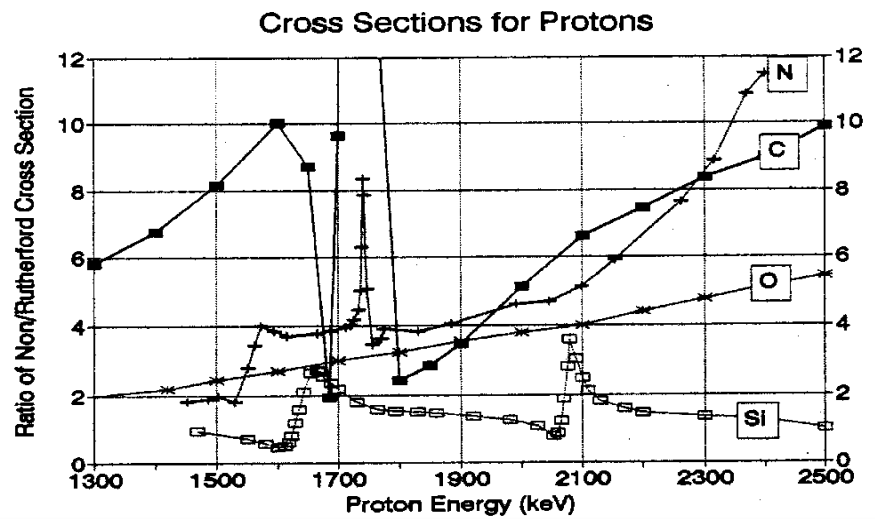


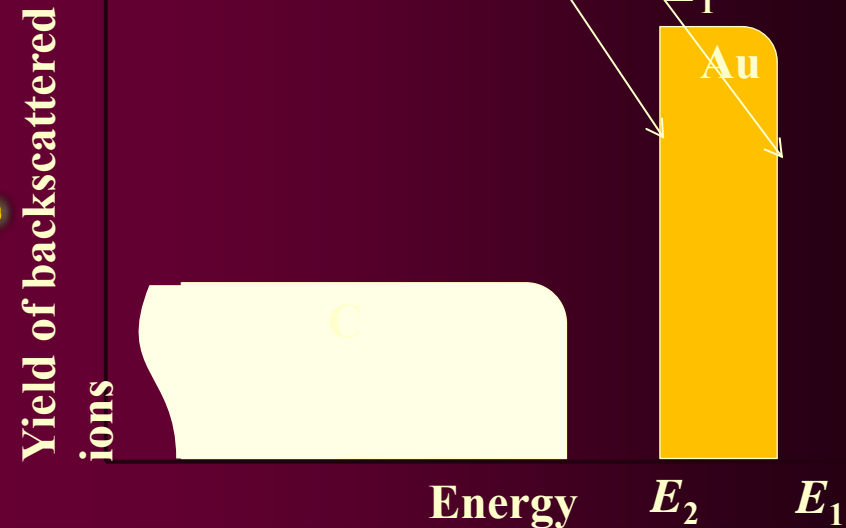
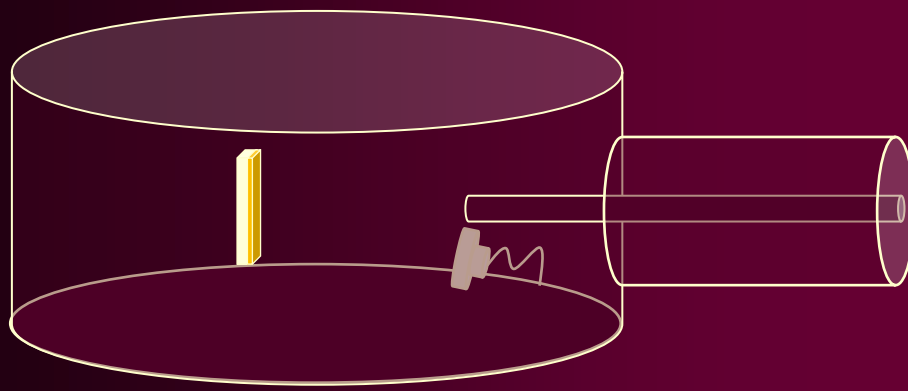
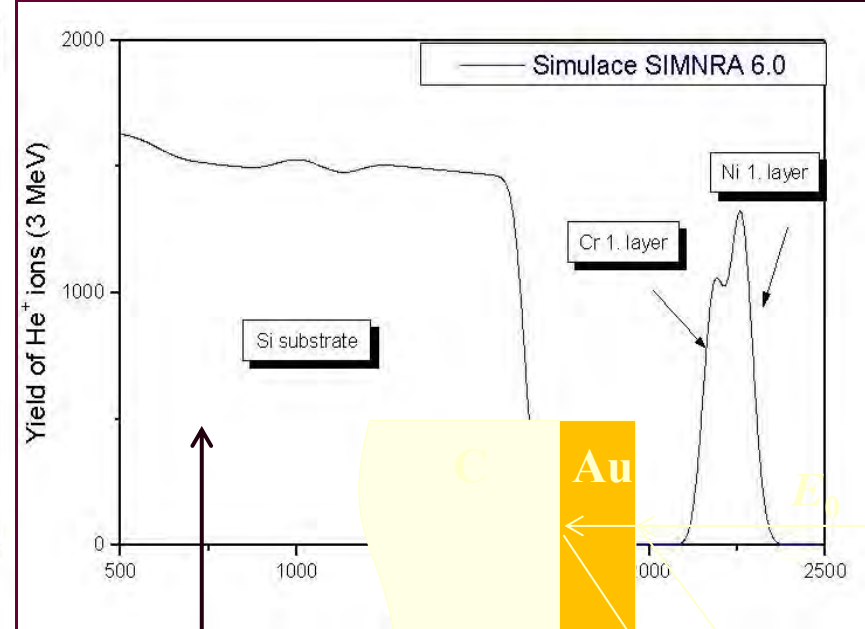
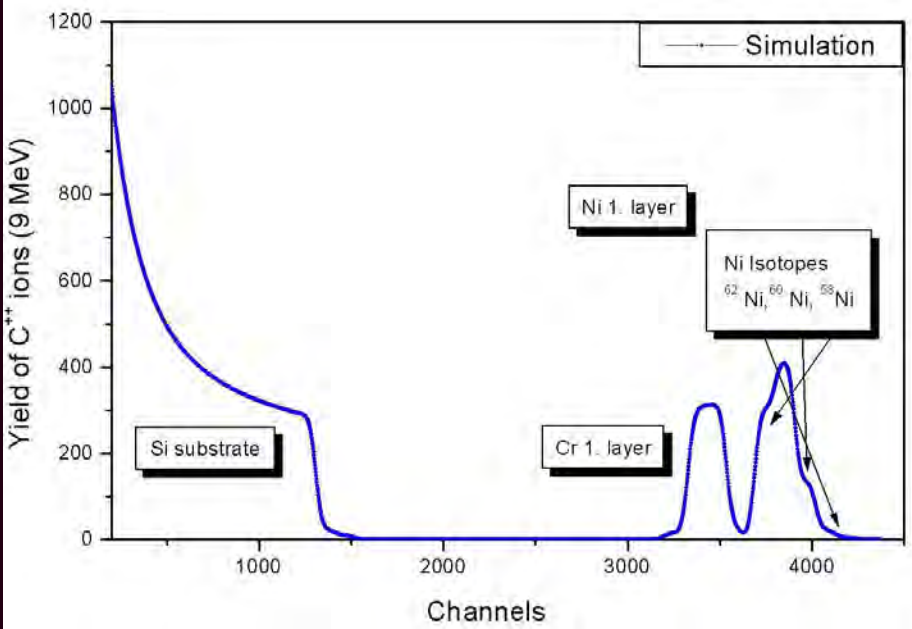
FIGURE 20. The $A + B \cdot E^{0.5}$ (keV) detector resolution of a standard silicon surface barrier detector for various ions as calculated from the parameters of Reference 131. The energy range plotted may exceed that of original experimental data.



ION BEAMS PROVIDED BY SMALL ACCELERATOR

HEAVY IONS - RBS

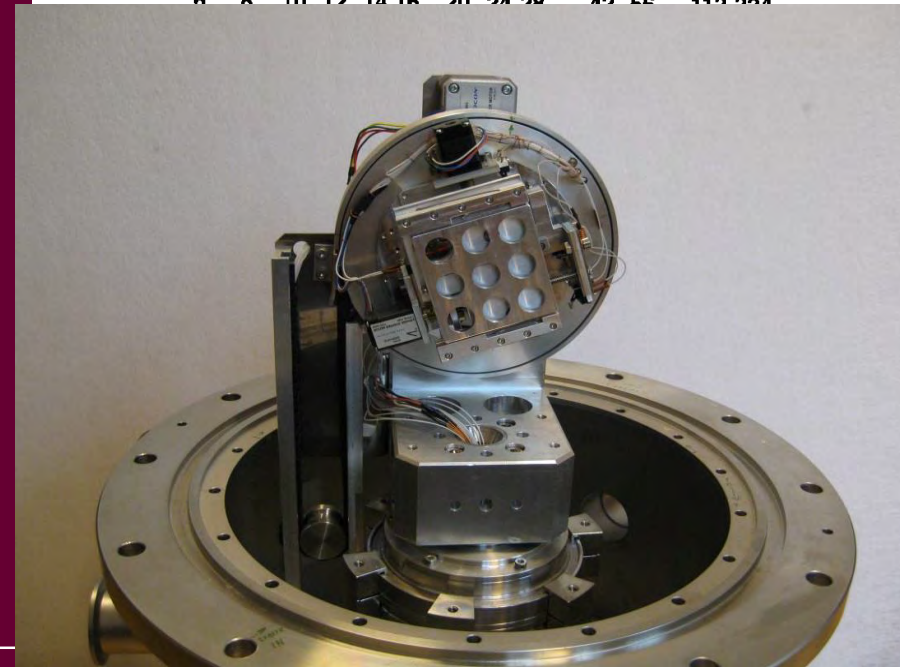
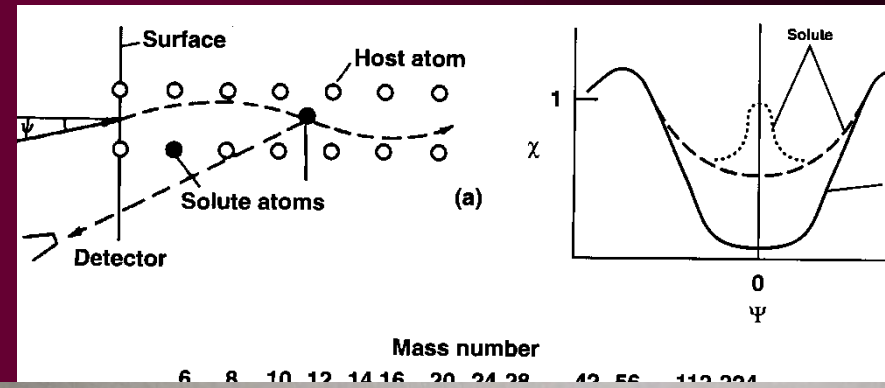
Heavy ions enable us to get the better mass resolution.



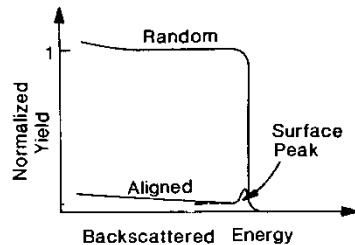
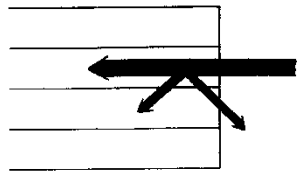
ION BEAMS PROVIDED BY SMALL ACCELERATOR

RBS- CHANNELING

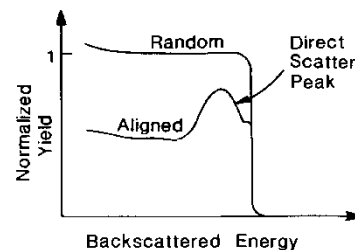
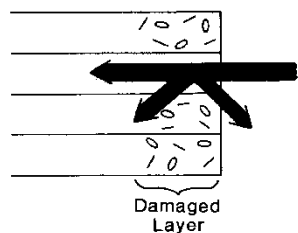
RBS-channeling spectrometry - enables us to investigate crystalline materials. The signal of the impurity and host lattice in RBS spectra is separated by scattering kinematics. The angular yield curve (scan) is obtained by monitoring the yield of the impurity and host lattice along the channeling axis using ion beam impact angle changing. From the angular yield curves of the axial channels in material we obtain the impurity position in the measured crystallographic direction. In order to determine the lattice position of impurities several relevant crystallographic directions have been selected.



a) PERFECT CRYSTAL



b) IMPERFECT CRYSTAL



$$\psi_c = \sqrt{\frac{U(r_{\min})}{E}}$$

$$\psi_c \approx 1^\circ$$

Lindhard theory

$$\chi_{\min} = Nd\pi\rho^2 \psi_c = (2Z_1Z_2e^2 / Ed)^{1/2}$$

Dechanneled yield of back-scattered ions

-- given by part of ions randomly redistributed

-- given by disordered atoms – disordered atoms density n_D

$$\chi_D(z)$$

$$\chi_R(z)$$

$$\chi_D(z) = \chi_R(z) + (1 - \chi_R) f \frac{n_D(z)}{n}$$

$$\chi_R(z) = \chi_V(z) + [1 - \chi_V(z)] \left[1 - \exp \left(- \int_0^z \delta_D n_D(z') dz' \right) \right]$$

- yield of ions in virgine crystal $\chi_V(z)$

dechanneling – parameter

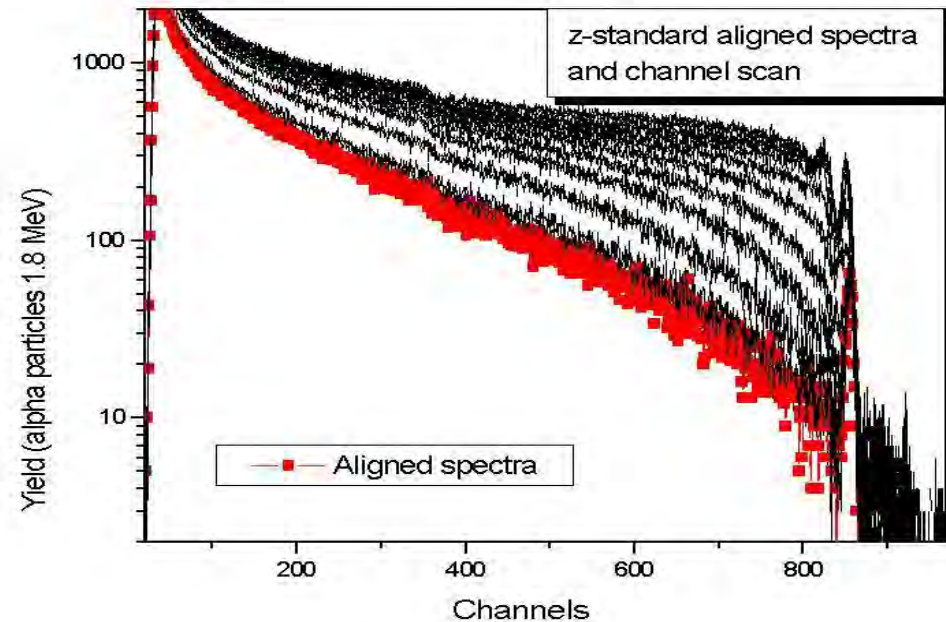
$$\delta_D \approx \frac{\pi}{2} \frac{Z_1 Z_2 e^2 d}{E}$$

E – ion energy

Z_1, Z_2 – projectile and lattice nuclei charge

d – lattice constant

The relative amount of the dislocated atoms for N_D/N is deduced from the equation $N_D/N = (\chi_D - \chi_V) / (1 - \chi_V)$, where χ_V is the minimum yield in the aligned virgin spectra and χ_D is the minimum yield in the aligned spectra of the implanted samples.

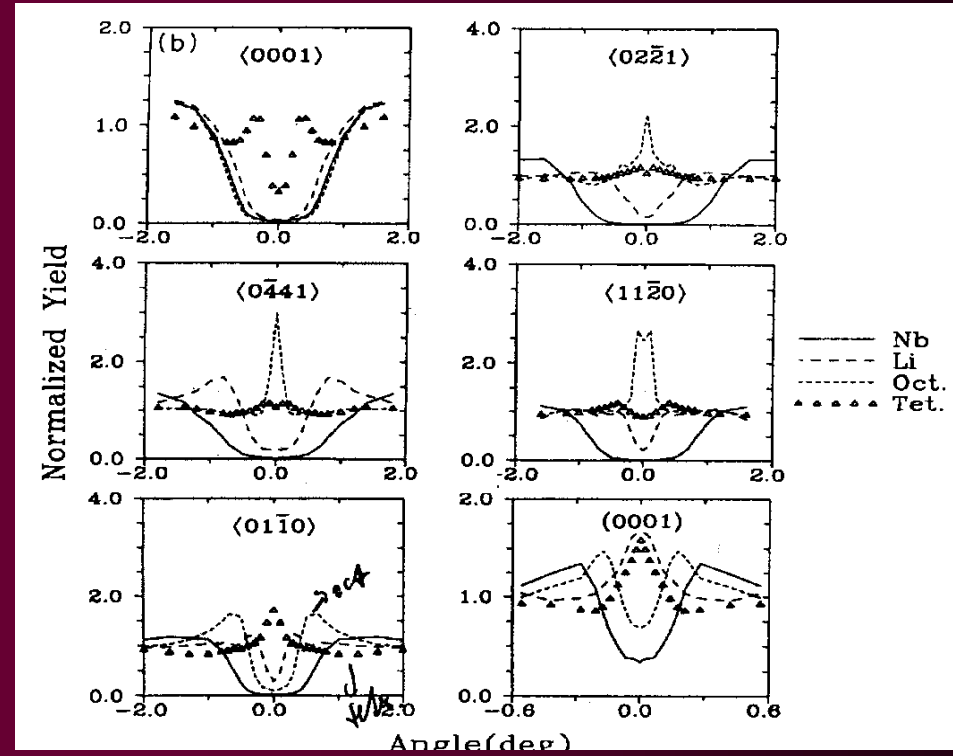
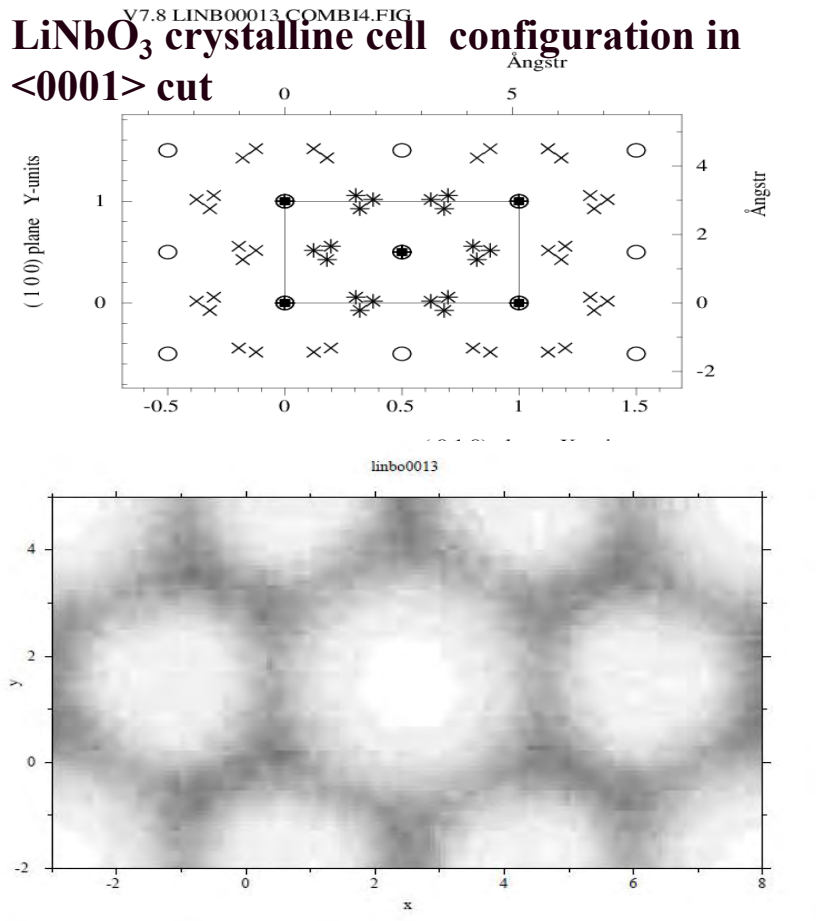


COMPUTER SIMULATIONS CHANNELING IONS IN LiNbO_3

MC simulation of the large number of ions incoming into the crystal lattice was performed. The string potential was used with taking into account the screened Thomas - Fermi potential.

- the binary collisions with the closest atoms should be taken into account
- the deflection caused by the string potential of the atoms
- the energy electronic losses, the angle straggling of the ions, the energy straggling
- the thermal vibrations of the crystal lattice (Gaussian isotropic distribution)

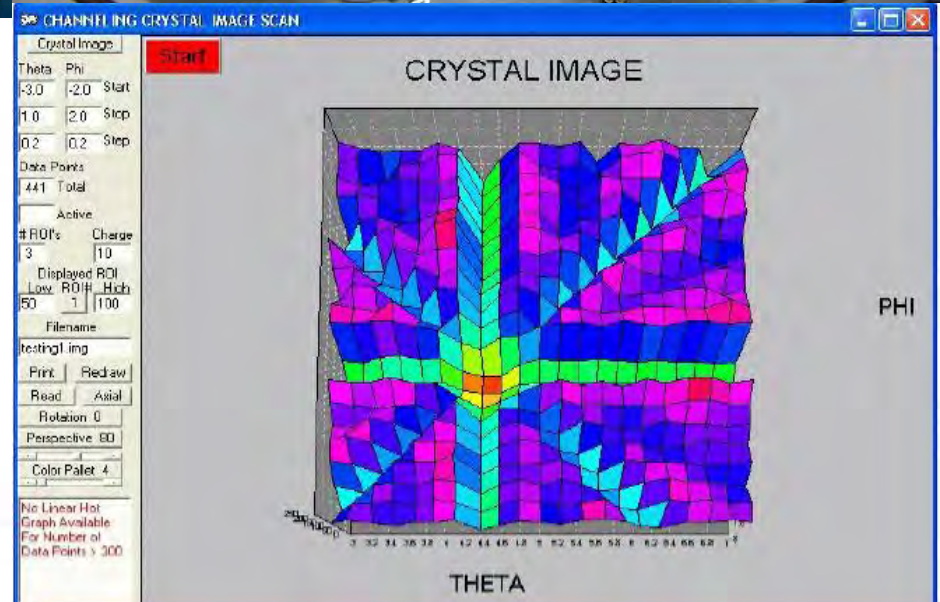
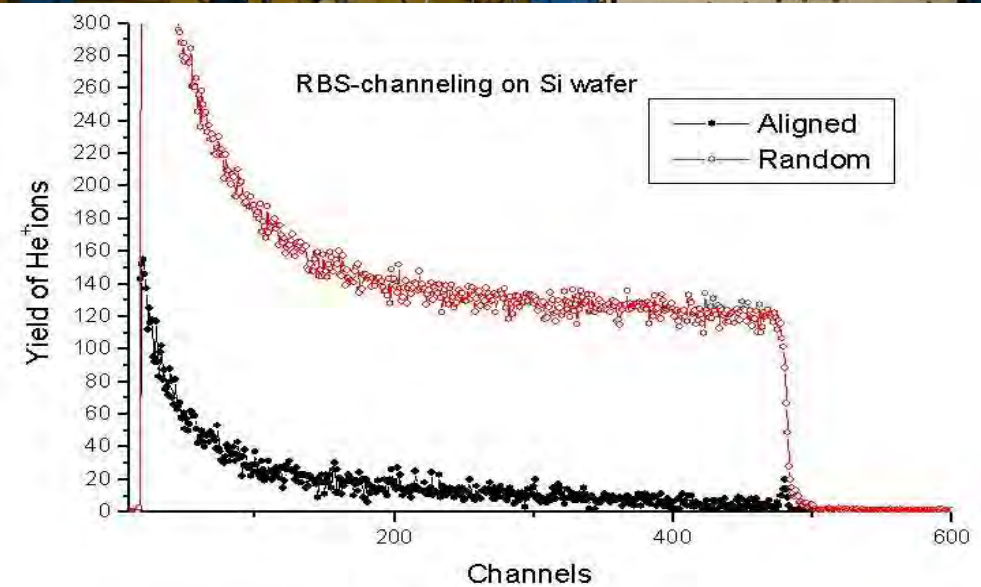
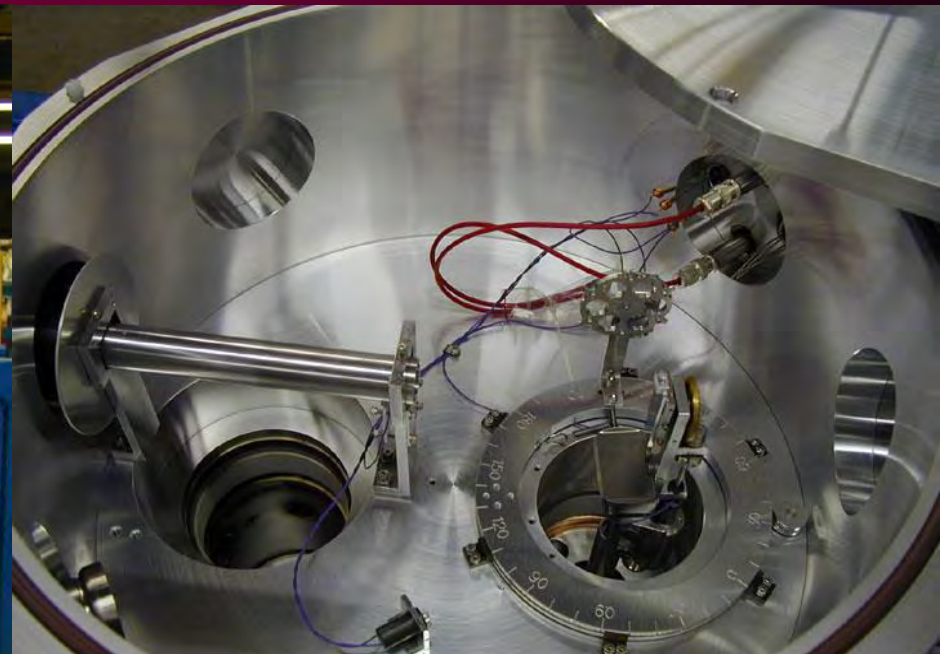
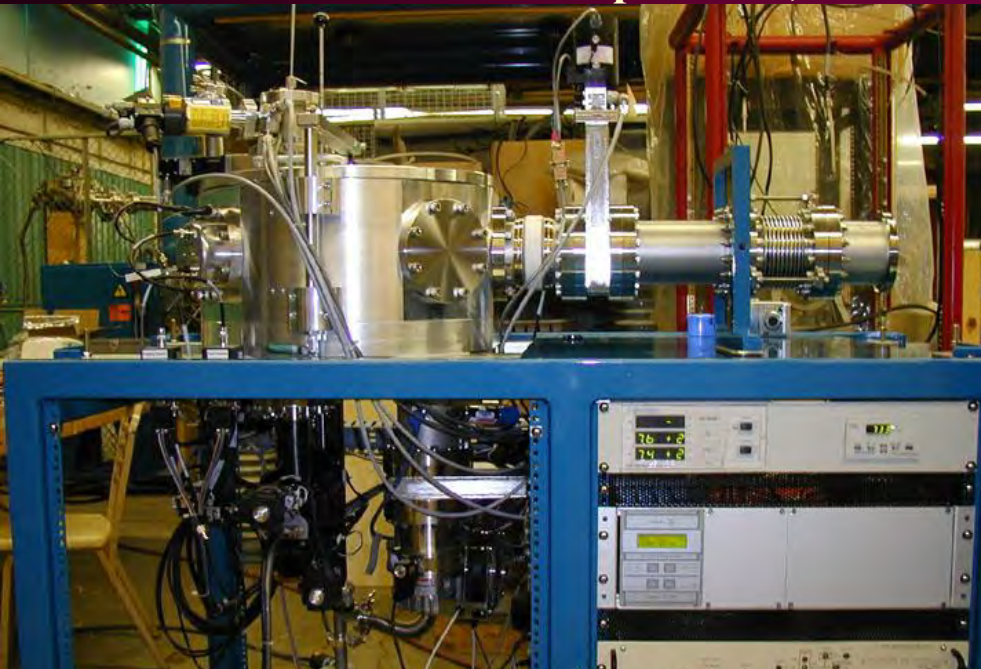
$$V(\vec{r}) = \frac{Z_1 Z_2 e^2}{\vec{r}} (0.1e^{-6\vec{r}/a} + 0.35e^{-0.3\vec{r}/a} + 0.55e^{-1.2\vec{r}/a})$$



L. Rebouta, P. J. , M. Smulders, D. Boerma, F. Agulló-Lopez, M. F. da Silva, J. C. Soares, Physical Review B, Vol.48, pp. 3600-3610, 1993.

RBS-CHANNELING - INSTRUMENTATION

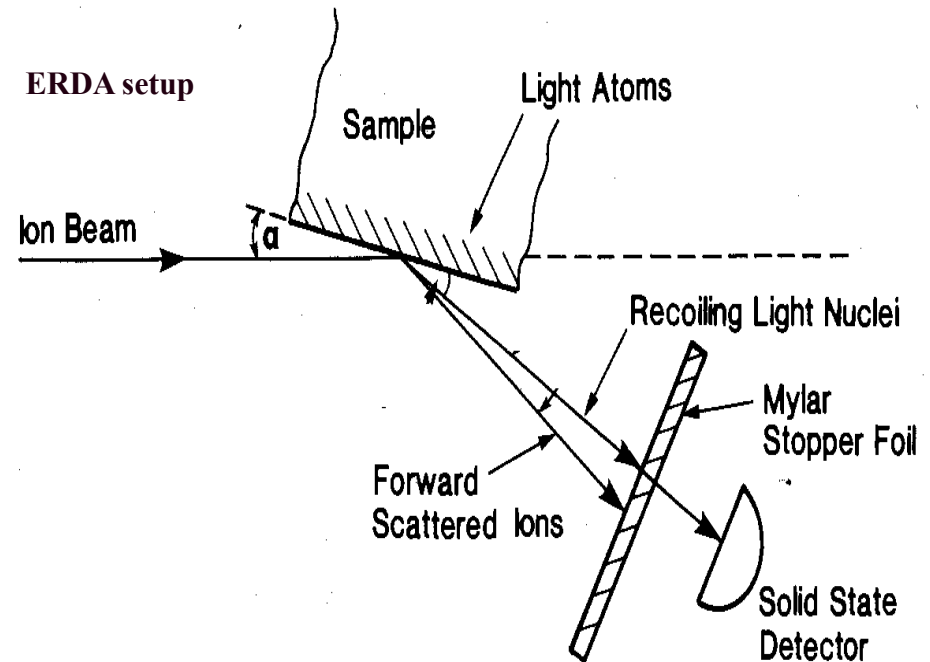
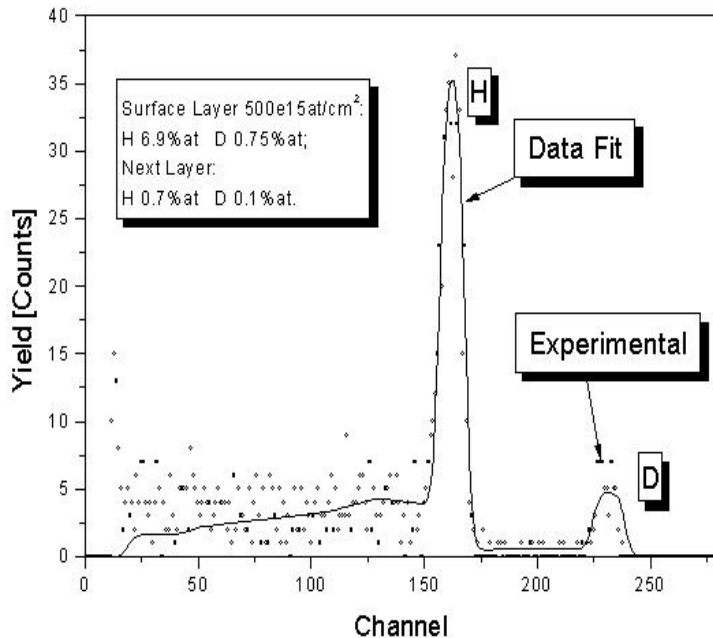
- National Electrostatics Corporation, USA



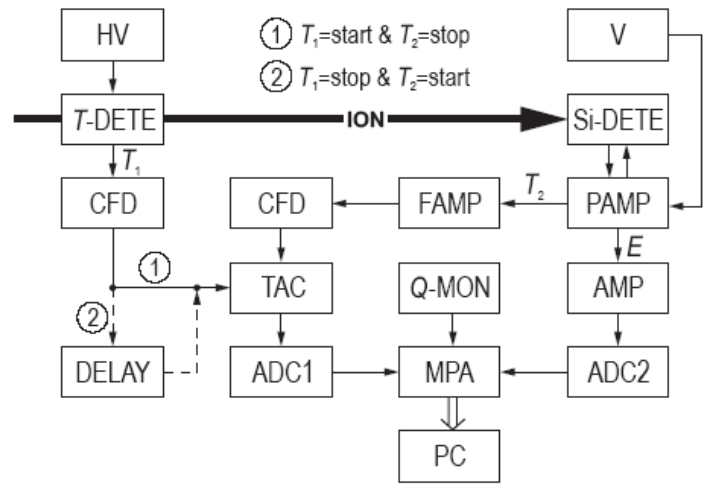
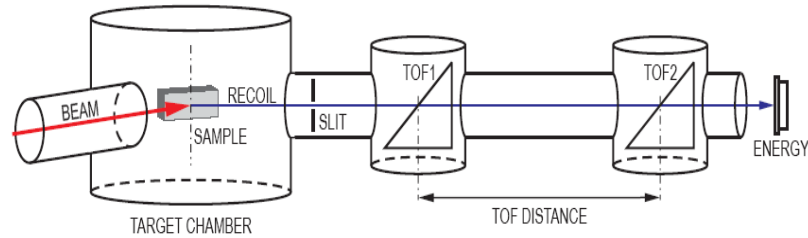
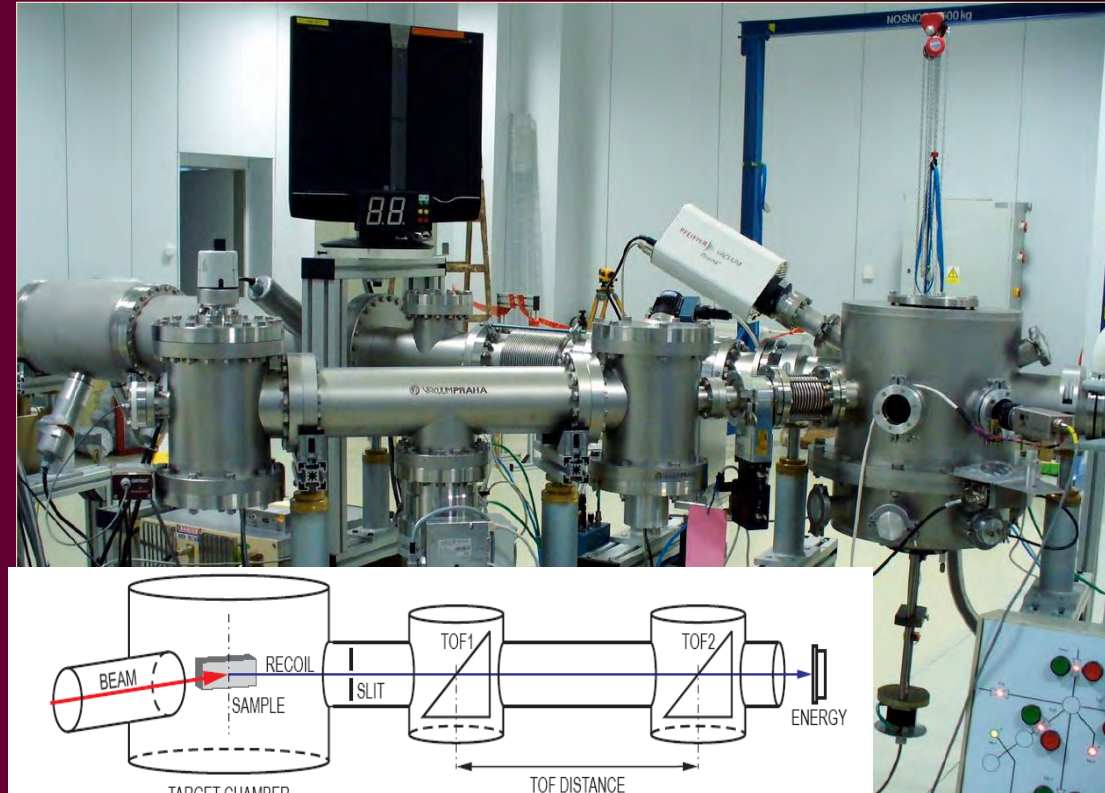
ION BEAMS PROVIDED BY SMALL ACCELERATOR

ELASTIC RECOIL DETECTION ANALYSIS - ERDA

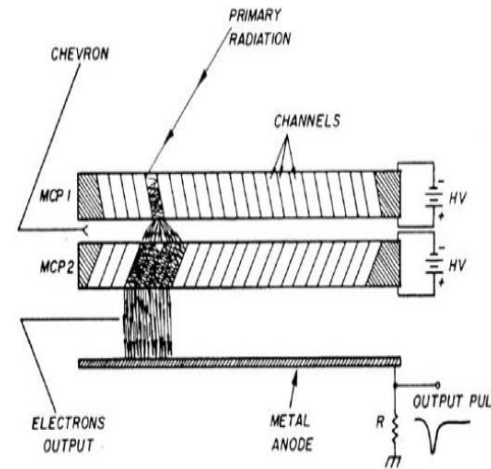
The elastic-recoil detection analysis (ERDA) is one of the IBA methods suited for the non-destructive depth profiling of light elements in bulk samples. It is based on the detection of atoms which are knocked out from the sample by incoming heavy ions. When only kinetic energy is measured, ions of different elements coming from various depth within the sample can produce the same signal in the energy detector. In addition, also elastically scattered primary ions can be detected which further complicate the acquisition and evaluation of the energy spectra. To overcome this difficulty Time-of-Flight ERDA (TOF-ERDA) was developed.



ERDA TOF



- HV ... Time detector high-voltage supply
- V ... Energy detector voltage supply
- T-DETE ... Time detector
- Si-DETE ... Energy detector
- CFD ... Constant-fraction discriminator
- FAMP ... Fast timing amplifier
- PAMP ... Preamplifier
- TAC ... Time-to-amplitude converter
- Q-MON ... Accumulated charge monitor
- AMP ... Amplifier
- DELAY ... Delay box
- ADC ... Analog-to-digital converter
- MPA ... Multi-parameter data acquisition system
- PC ... Personal computer



ION BEAMS PROVIDED BY SMALL ACCELERATOR

Measurement of the time of flight of ions through the TOF telescope serves for distinguishing the outgoing ions and recoiled atoms according to their mass. The time of flight t is given by the non-relativistic formula.

$$t = l \sqrt{\frac{m}{2(E_{out} - E')}}$$

l ... Fixed distance of flight

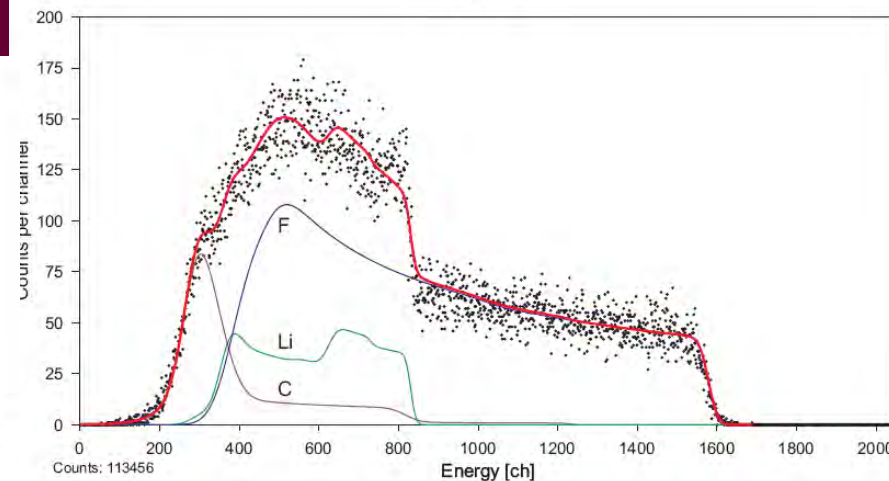
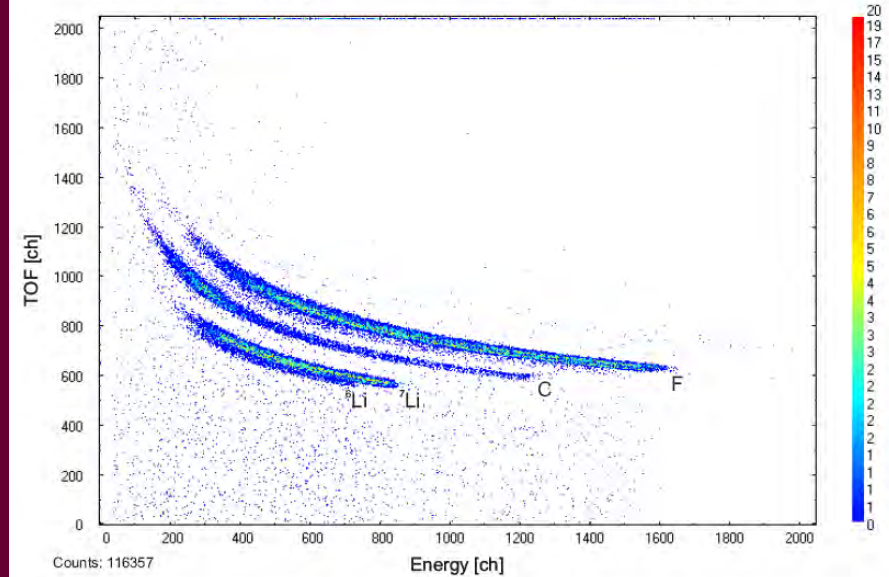
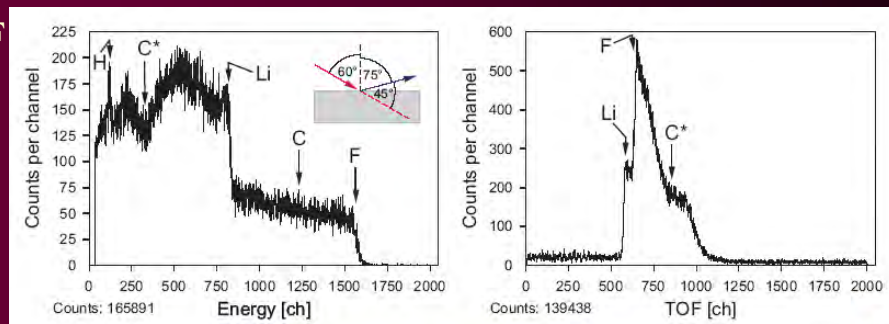
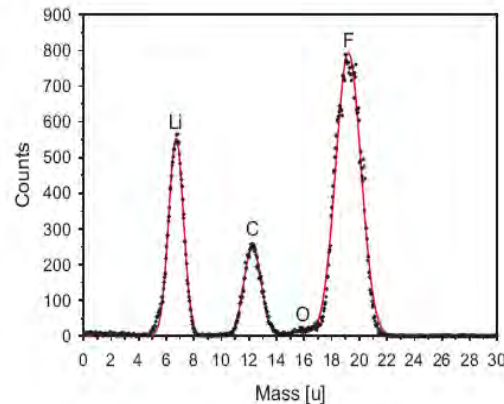
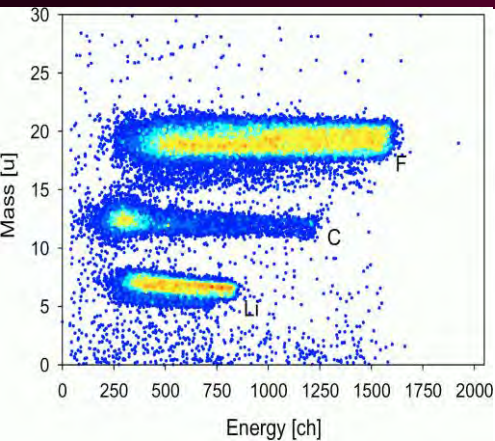
m ... Recoiled atom mass

E' ... energy loss of recoiled atom in the time detector

Testing of TOF spectrometer

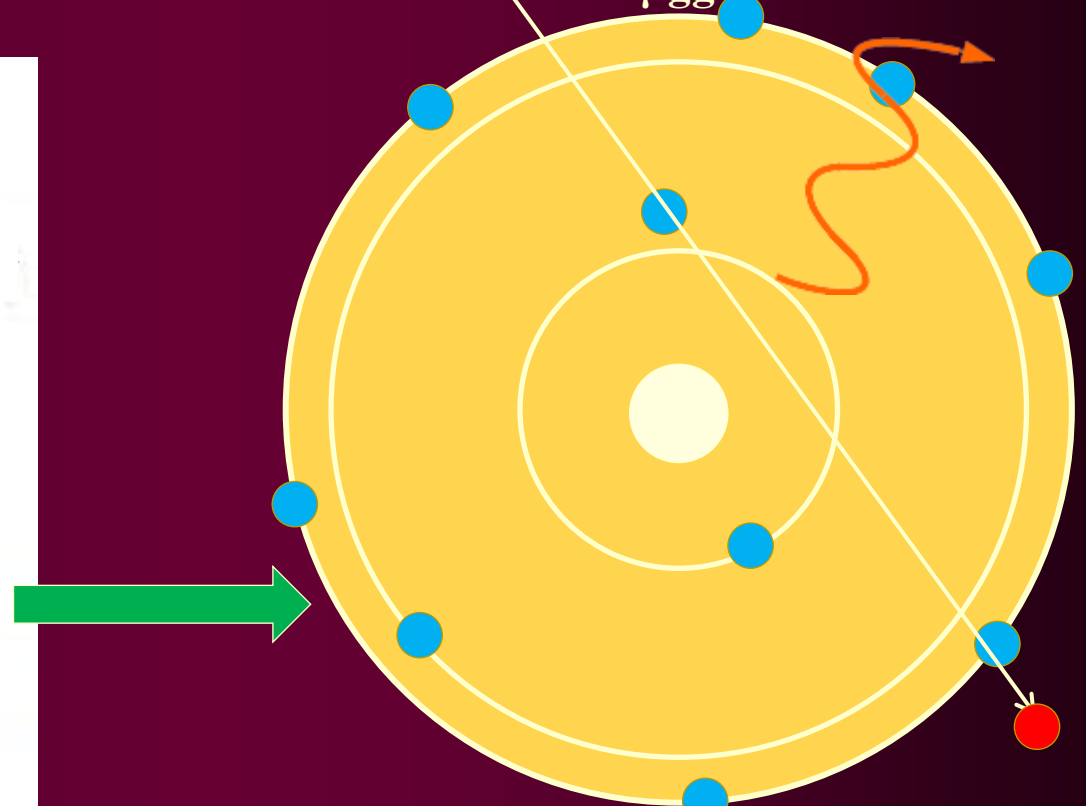
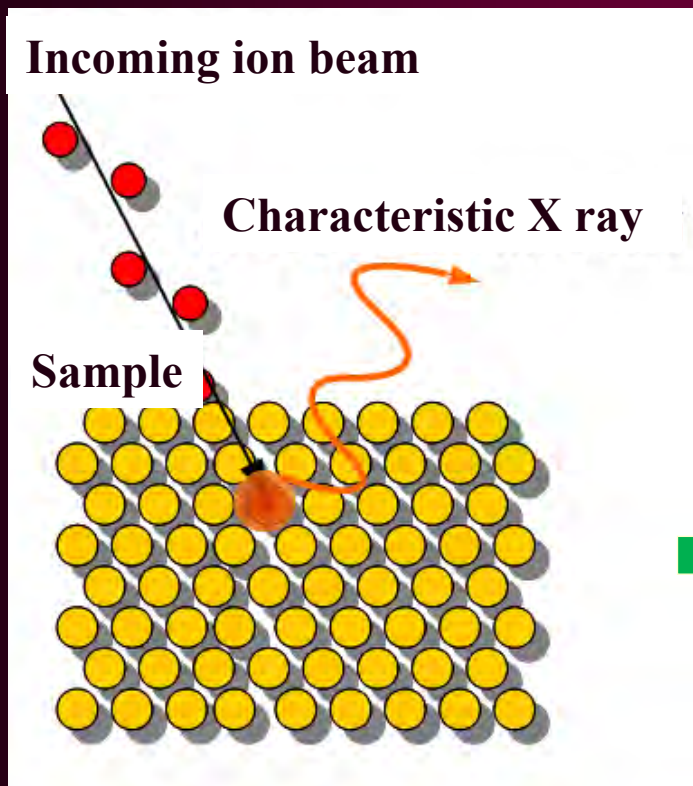
Used parameters

- ion beam: 15,4 MeV Cu^{6+} (terminal voltage: 2,2 MV)
- Used sample: 200 nm LiF layer deposited on glassy carbon



PARTICLE INDUCED X-RAY EMISSION SPECTROSCOPY (PIXE)

- PIXE uses X-ray emission for elemental analysis . Samples are irradiated by an ion beam from an accelerator and characteristic X-rays are then detected.
- Ions, or protons, with energies of a few MeV ionize atoms in the sample and induce the emission of characteristic X-rays.
- The X-ray yield depends on the number of atoms in the sample, the ionization cross section, the intensity of the ion beam.
- Depending on the sample type and measuring apparatus, the concentration of elements with $Z > 5$ can be determined with sensitivities of $0.1\text{--}1 \mu\text{g g}^{-1}$.



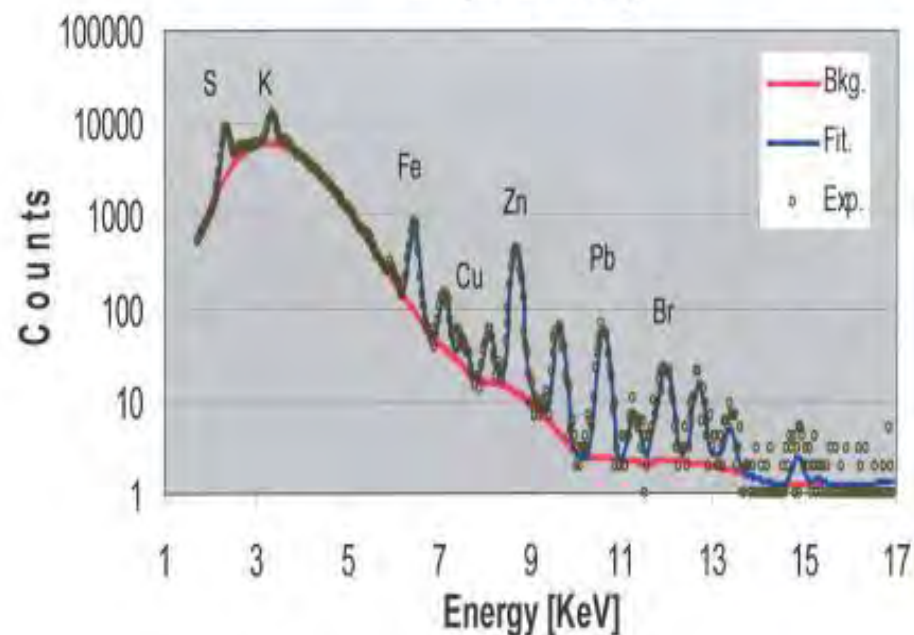
ION BEAMS PROVIDED BY SMALL ACCELERATOR

PIXE AND NRA

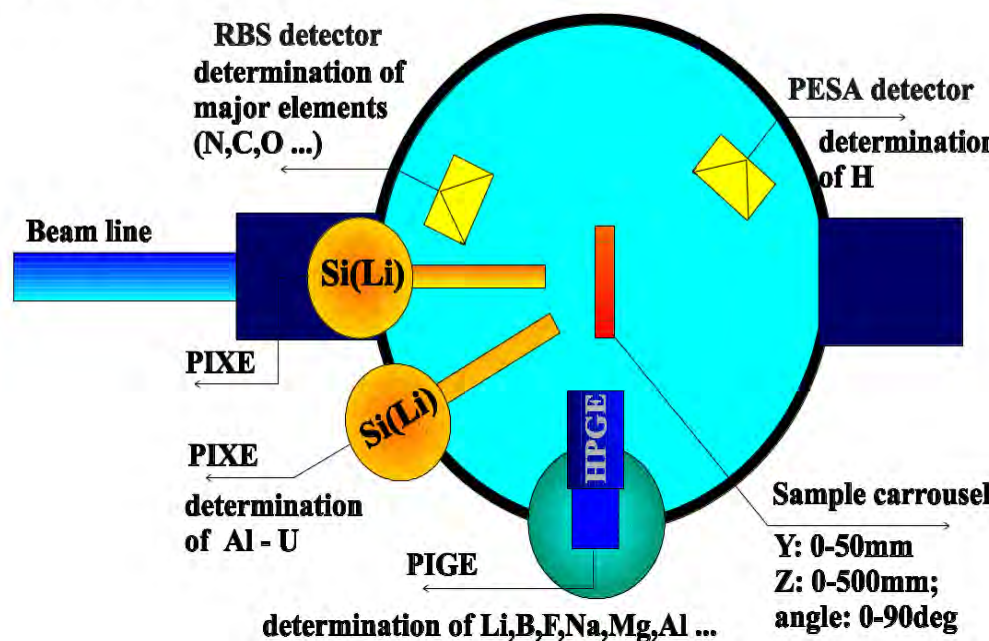
Nuclear reaction methods are suitable for identifying a range of isotopes from ^1H to ^{32}S . The most frequently used reactions are (p, α), (d,p), and (d, α) which provide useful alternative methods for determining isotopes such as ^2D , ^{12}C , and ^{16}O , compared with Rutherford Back-Scattering spectrometry (RBS) or Elastic Recoil Detection Analysis (ERDA).

Isotopes up to ^{32}S can be determined in heavier matrices at mgg^{-1} levels depending on the maximum beam current that the sample can withstand. The use of glancing measurement geometries or heavy incident ions make possible depth profiling with typical resolutions at the surface of 10–100 nm.

The PIXE spectrum of the BLPI impactor sample
one spot from the stage 5



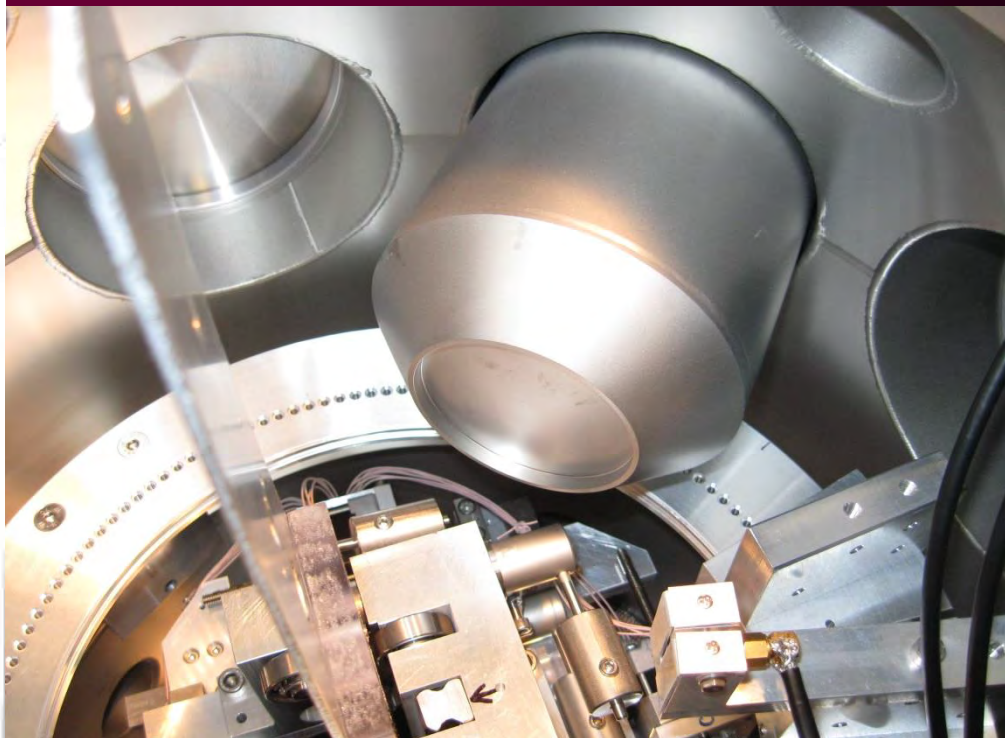
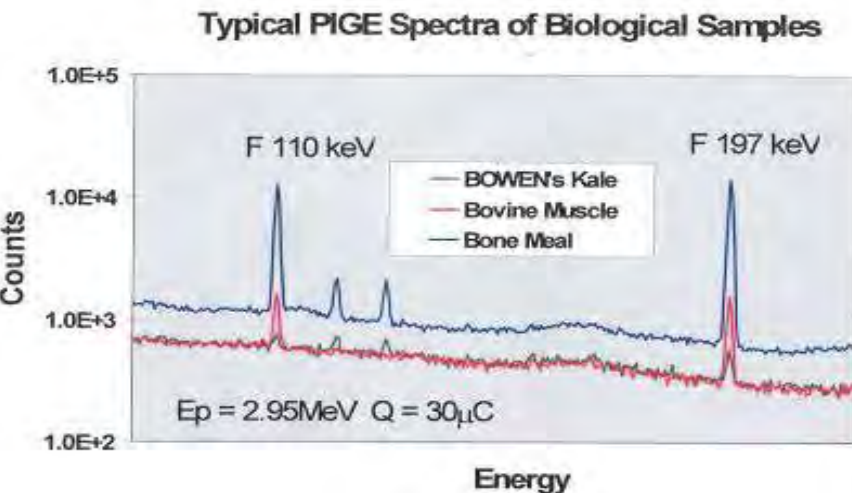
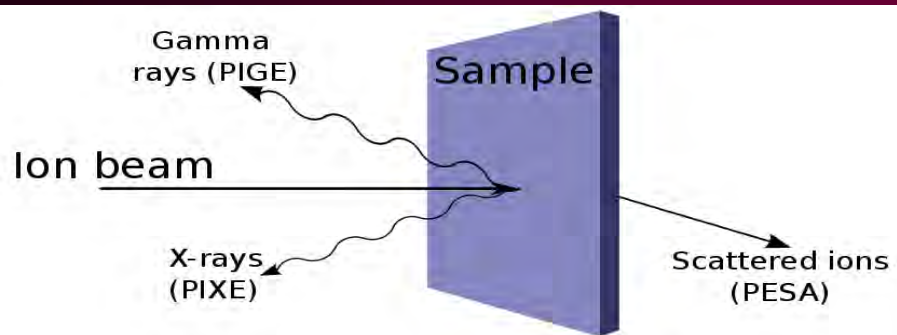
Experimental chamber for simultaneous analyses
by PIXE, RBS, PESA and PIGE



ION BEAMS PROVIDED BY SMALL ACCELERATOR

PIGE INSTRUMENTATION

- PIGE (particle-induced gamma-ray emission) is a versatile non-destructive analytical and depth profiling technique based on the (p, γ) reaction. The energy and intensity of the γ -ray lines indicate the elements that are present and their amounts, respectively.
- For protons with energies from 1 to 3MeV, the best sensitivities are found for Li, B, F, Na, and Al.
- The highest cross sections are for light isotopes ($A < 30$), which can be determined with a sensitivity of $1 \mu\text{g}^{-1}$ or less.

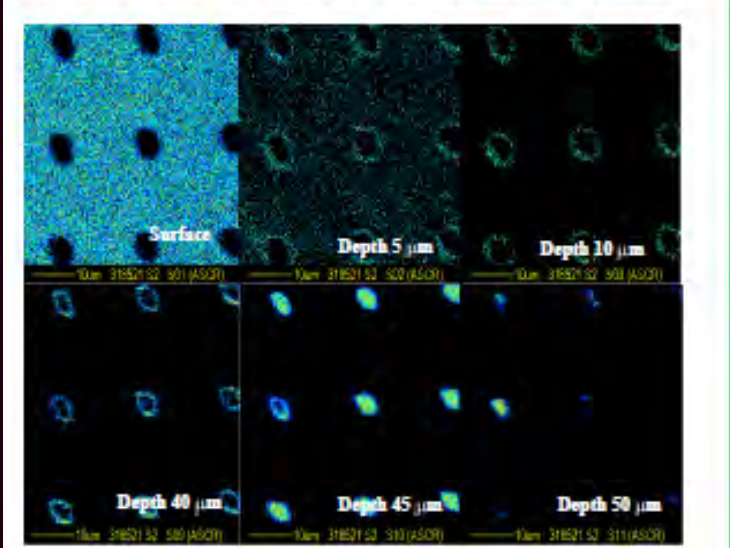


ION BEAMS PROVIDED BY SMALL ACCELERATOR

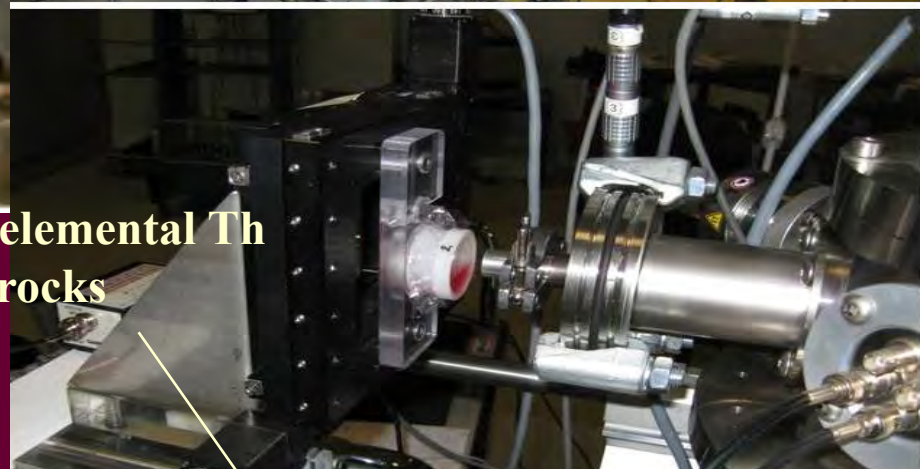
ION MICROPROBE AND EXTERNAL BEAM



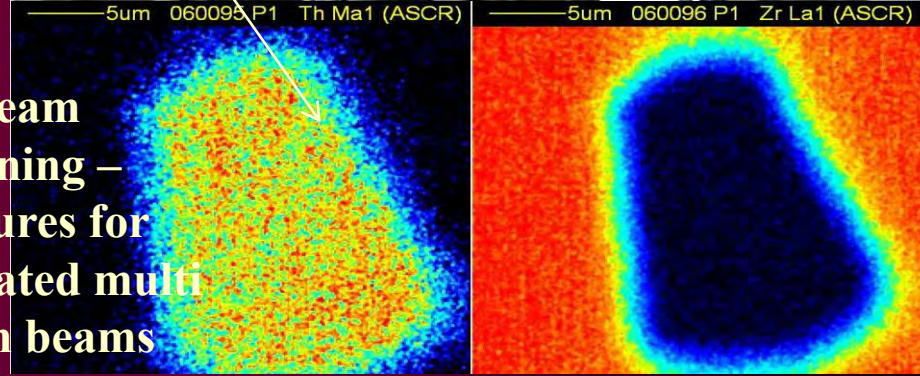
In Fig. 7 are exhibited maps of the two dimensional scan indicating the shape of the holes at different depth written in the resist. 1 mm x 1 mm pattern, scan size 50 μm x 50 μm , of 50 μm PMMA foil irradiated at $3.75 \cdot 10^{14}$ protons/cm² fluence. PMMA was nearly fully removed.



Microbeam elemental Th mapping in rocks for nuclear waste disposal

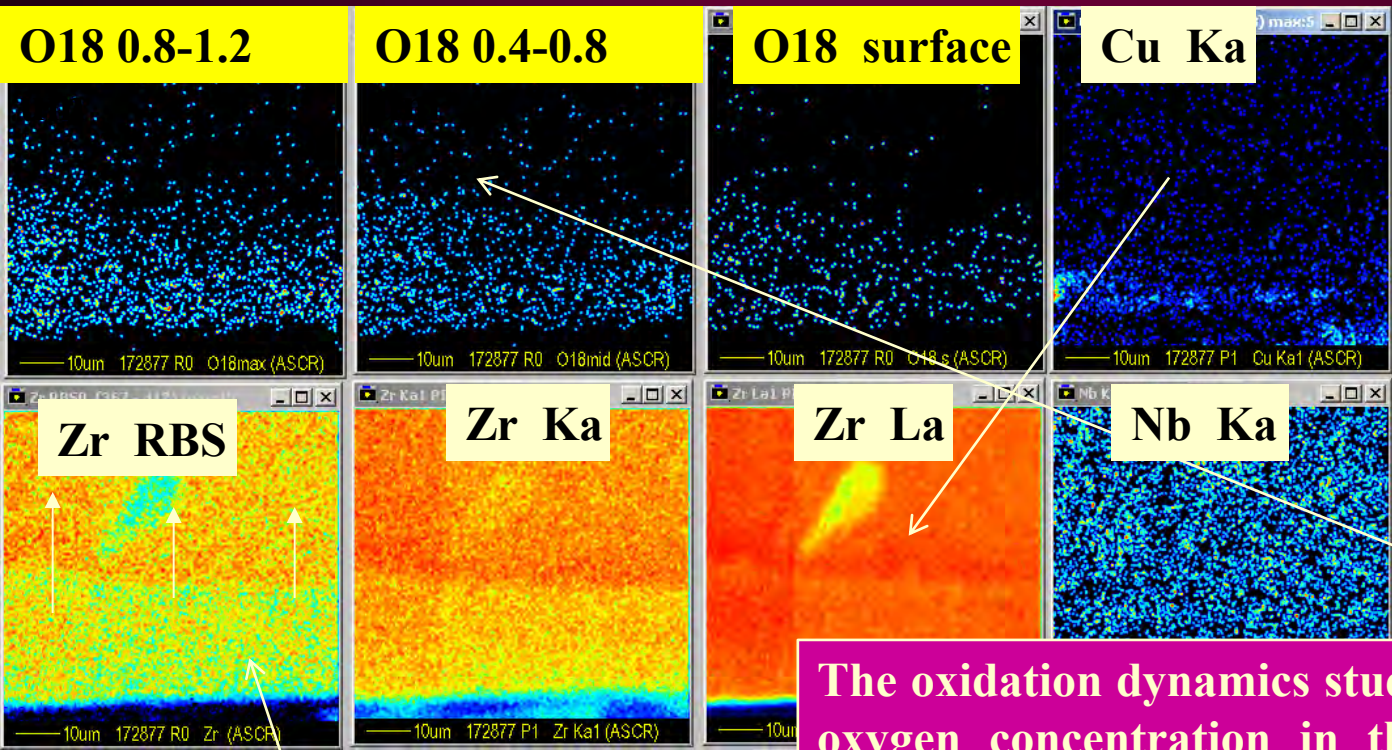


Heavy ion beam micromachining – microstructures for Laser generated multi energetic ion beams



ION BEAMS PROVIDED BY SMALL ACCELERATOR

ION MICROBEAM FOR NUCLEAR TECHNOLOGY

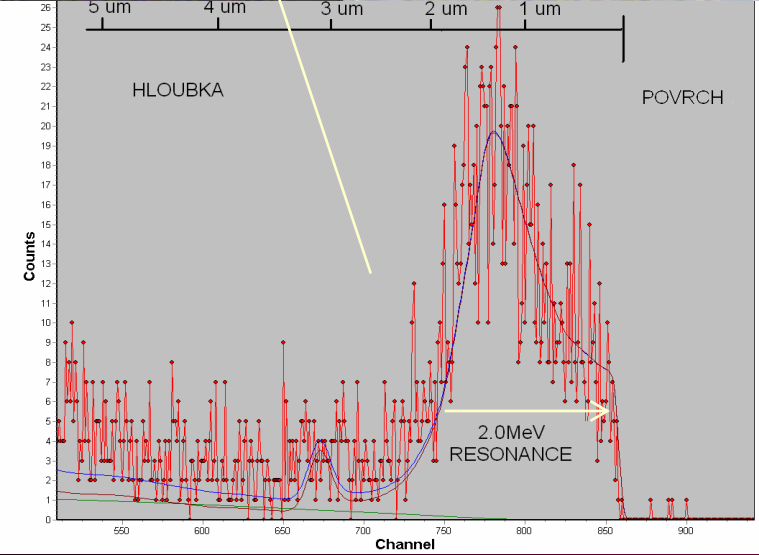


3D elemental mapping

- Oxidation study of Zr alloys
- Oxidation in ^{16}O and afterwards in ^{18}O

Used ion beam
 H^+ ions, $E = 2050\text{keV}$
 1 h 40 min, scan 75 x nuclear

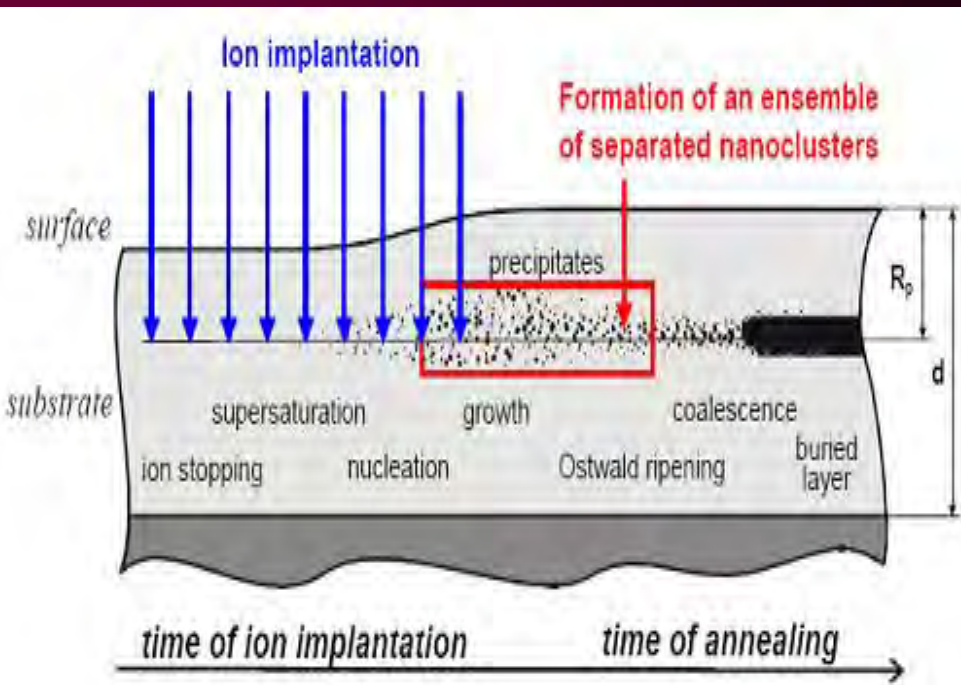
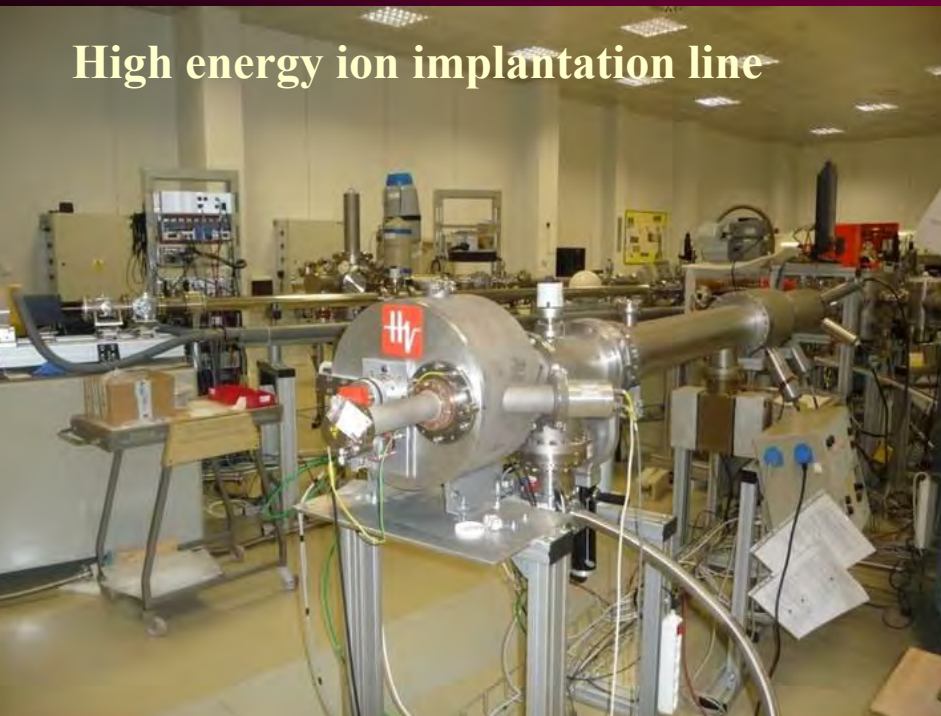
The oxidation dynamics study, different oxygen concentration in the different depths, RBS gives information about the oxygen depth distribution, while the nuclear reaction separates information about ^{18}O concentration, the oxidation is observed at grain boundaries.



	^{16}O	^{18}O
1 (11 x 50 μm) ZrO ₂	58 %	42 %
2 (11 x 50 μm) ZrO ₂	18 %	82 %
3 (30 x 30 μm) Zr	1.7 %	?

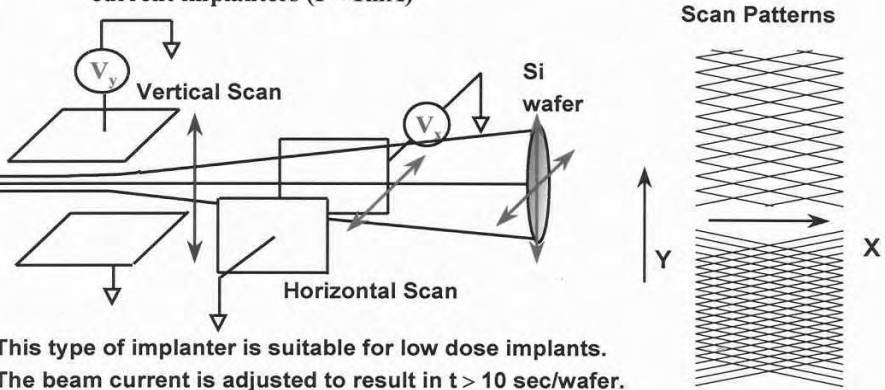
ION IMPLANTATION

High energy ion implantation line



Beam Scanning

Electrostatic scanning (low/medium beam current implanters ($I < 1\text{ mA}$))

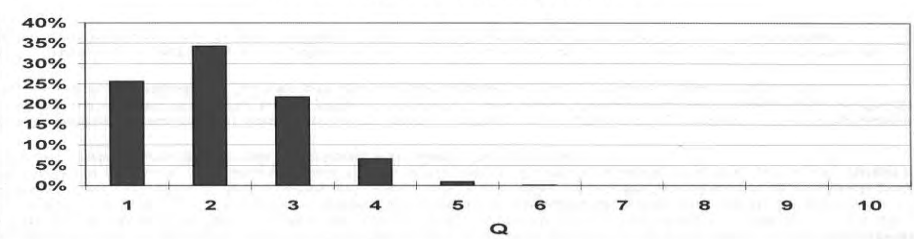


This type of implanter is suitable for low dose implants. The beam current is adjusted to result in $t > 10$ sec/wafer. With scan frequencies in the 100 Hz range, good implant uniformity is achieved with reasonable throughput.

Production of Au ions Different charge states

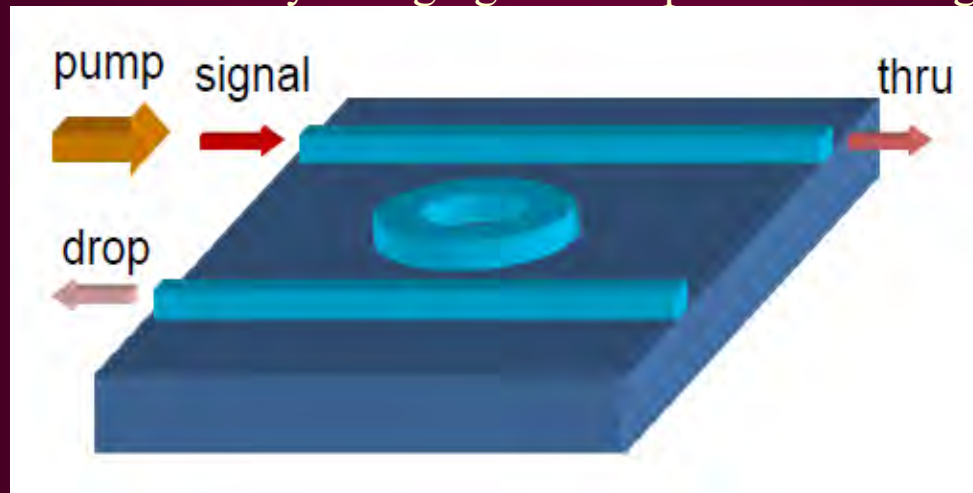
Q	fraction	MeV	ME/Q ²
1	26%	6	1182
2	34%	9	443
3	22%	12	263
4	7%	15	185
5	1%	18	142
6	0%	21	115
7	0%	24	96
8	0%	27	83
9	0%	30	73
10	0%	33	65

Gas Stripper Charge Distribution



NANOSTRUCTURES IN CRYSTALS AND GLASSES

- Nanocomposite glasses containing metal or semiconductor nanoparticles in glass matrix have promising utilisation in optoelectronics and photonics as all-optical devices.
- The presence of metal nanoparticles leads to an increase in nonlinear optical response, which is caused by surface plasmon resonance. Due to the Kerr optical effect, the typical values of the nonlinear refraction index can be increased from $10^{-18} \text{ cm}^2 \text{ W}^{-1}$ (undoped silica glass)
- The resulting nonlinear optical properties of nanocomposite materials depend on the size, shape as well as distribution of the embedded metal nanoparticles.
- Concerning the nucleation of Ag nanoparticles in the glass, it is well known that precipitation occurs mainly during high-ion-fluence implantation.
- At lower ion fluence, the precipitation of Ag nanoparticles can be supported by increasing the energy of the implanted ions or by changing the composition of the glass matrix.

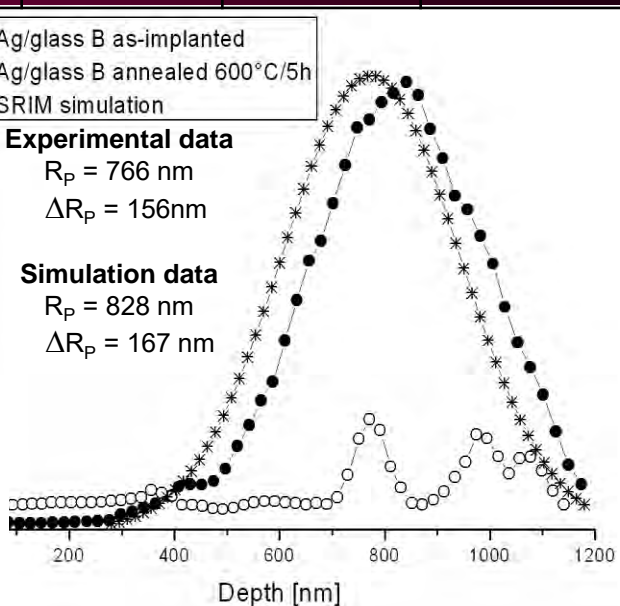
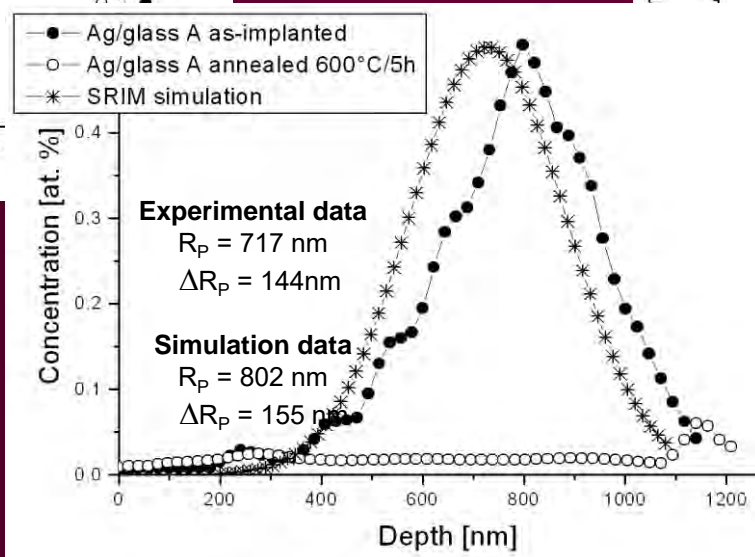
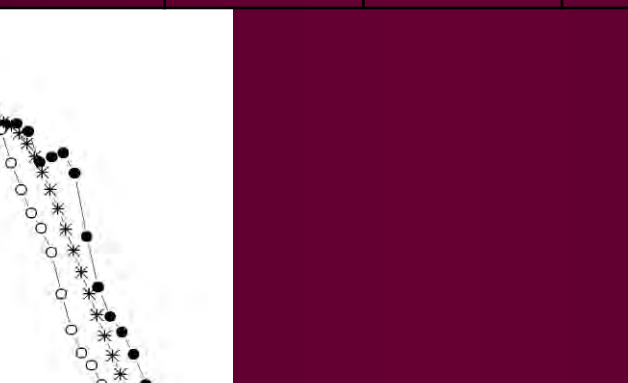
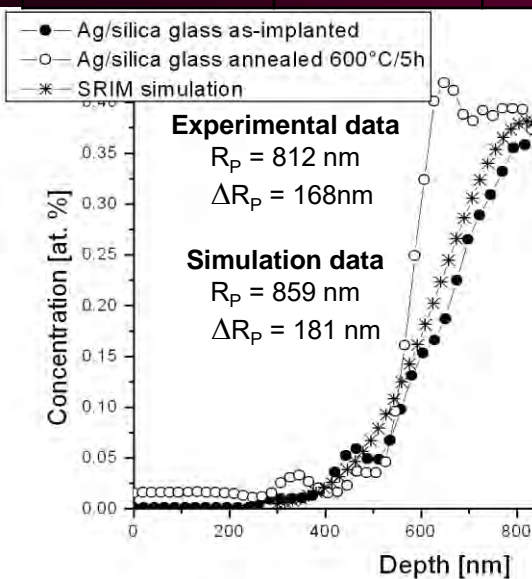


P. NEKVINDOVA, B. SVECOVA, J. CAJZL, A. MACKOVA, P. MALINSKY, J. OSWALD, A. KOLISTSCH, J. SPIRKOVA, Erbium ion implantation into different crystallographic cuts of lithium niobate, *Optical Materials*, Vol. 34, Issues , (2012) p. 652–659.

NANOSTRUCTURES IN CRYSTALS AND GLASSES

The chemical composition of the silica glasses used as a host matrix for metal nanoparticles [in at. %].

Substrate	Density [g·cm ⁻³]	Si [at %]	Na [at %]	Al [at %]	Ca [at %]	Mg [at %]	K [at %]	O [at %]
Glass A	2.49	25	10	0.5	2	2	0.2	60
Glass B	2.32	31	3	1.2	0.004	-	-	65
Silica glass	2.2	33.33	-	-	-	-	-	66.67

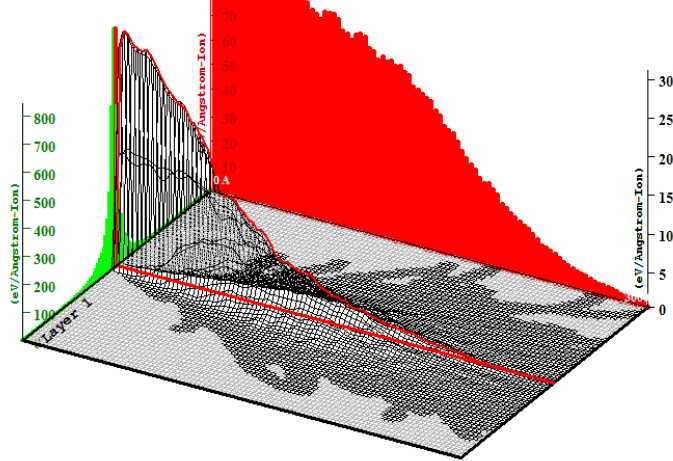


Various silica-based glasses were implanted with 1.7 MeV Ag⁺ ions with fluences of $1 \times 10^{16} \text{ cm}^{-2}$ and annealed at 600 °C for 5 hours.

NANOSTRUCTURES IN CRYSTALS AND GLASSES

Target Ionization

Total Ionization = 155.6 keV / Ion
 Total Phonons = 166.0 keV / Ion
 Total Target Damage = 8.39 keV / Ion

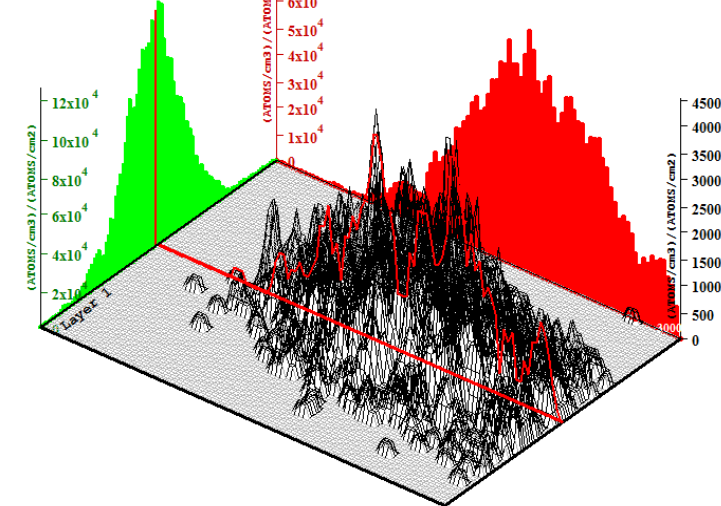


Plot Window goes from 0 Å to 3000 Å; cell width = 30 Å
 Press PAUSE TRIM to speed plots. Rotate plot with Mouse.

Ion = Ag (330. keV)

Ion Distribution

Ion Range = 1978 Å Skewness = 0.213
 Straggle = 515 Å Kurtosis = 2.372



Plot Window goes from 0 Å to 3000 Å; cell width = 30 Å
 Press PAUSE TRIM to speed plots. Rotate plot with Mouse.

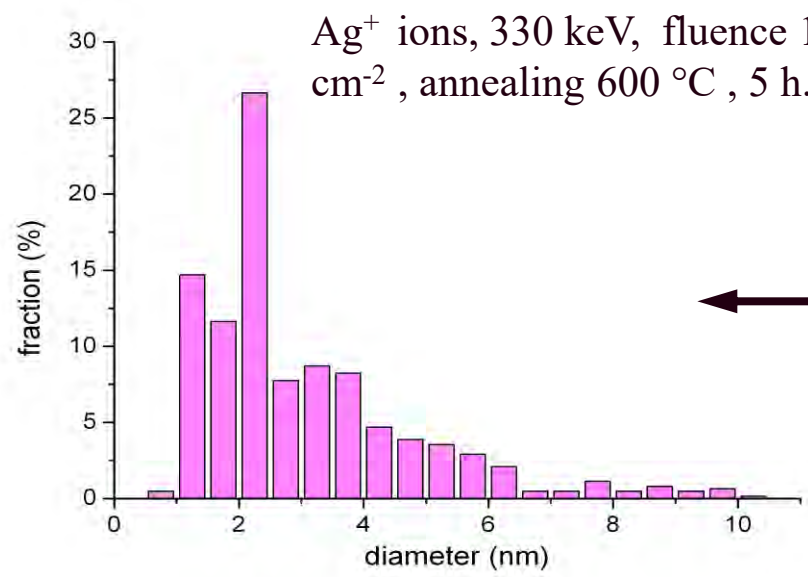
Ion = Ag (330. keV)

— Experimental
 — Simulated

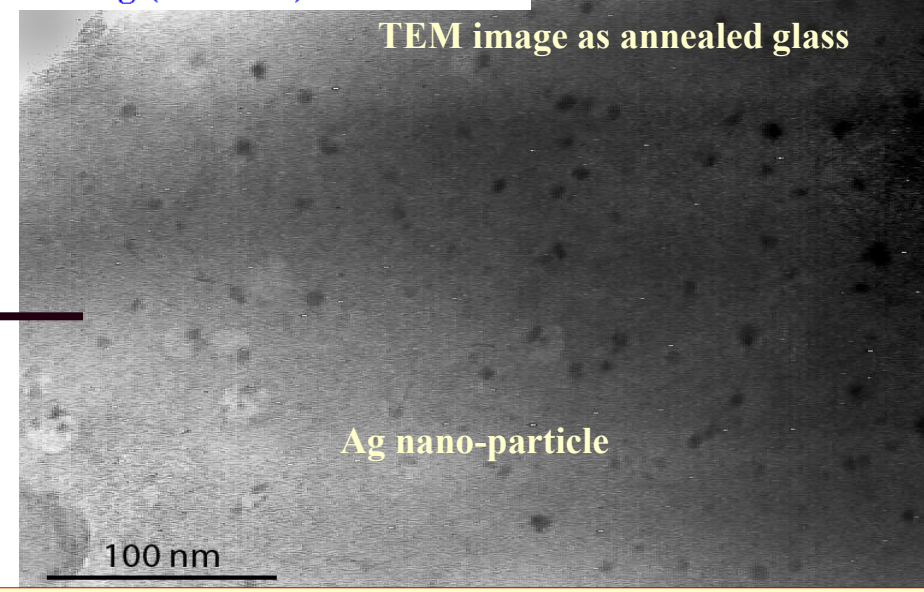
Au dose implanted
 1×10^{16} ions/cm²



nnels



Ag⁺ ions, 330 keV, fluence 1×10^{16} cm⁻², annealing 600 °C, 5 h.



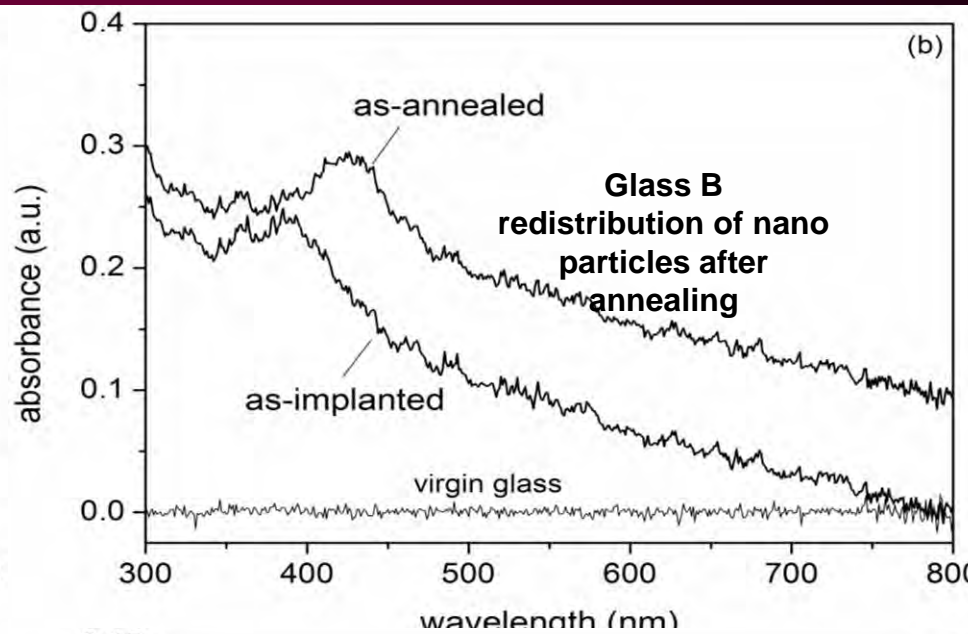
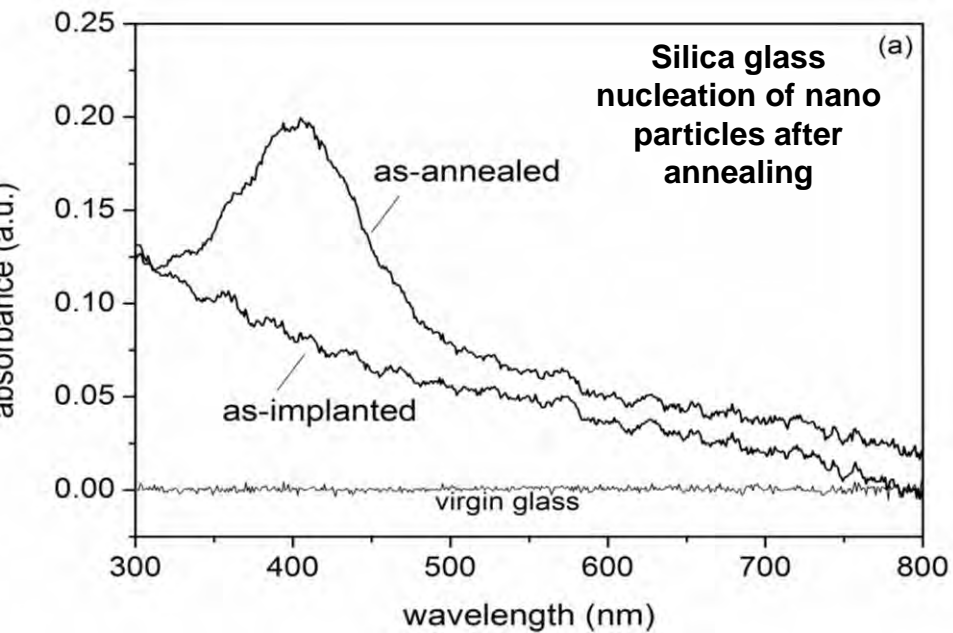
TEM image as annealed glass

Ag nano-particle

100 nm

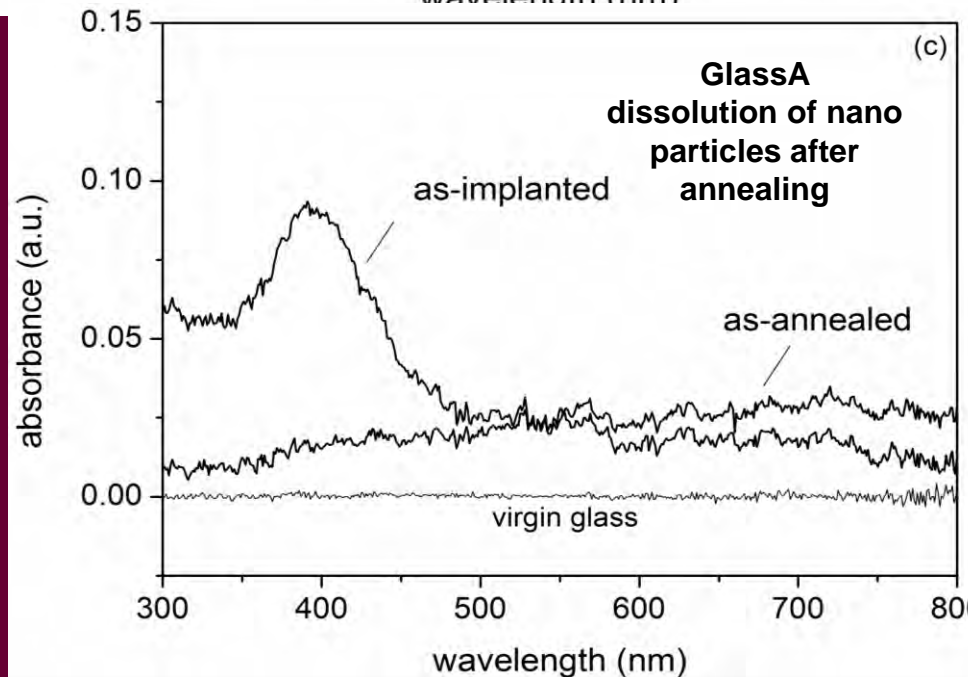
ION BEAMS PROVIDED BY SMALL ACCELERATOR

NANOSTRUCTURES IN CRYSTALS AND GLASSES



UV-VIS spectra were collected at ICHT using a CARY 50 dual beam spectrometer in transmission modes in the range from 300 to 800 nm.

Glasses A and B became yellow after the ion implantation, the absorption maxima were observed at 390 and 380 nm. In silica glass maximum appears at 400 nm.

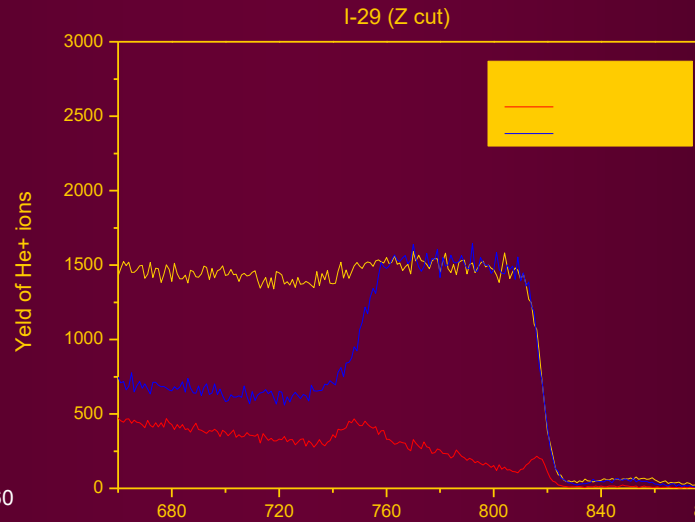
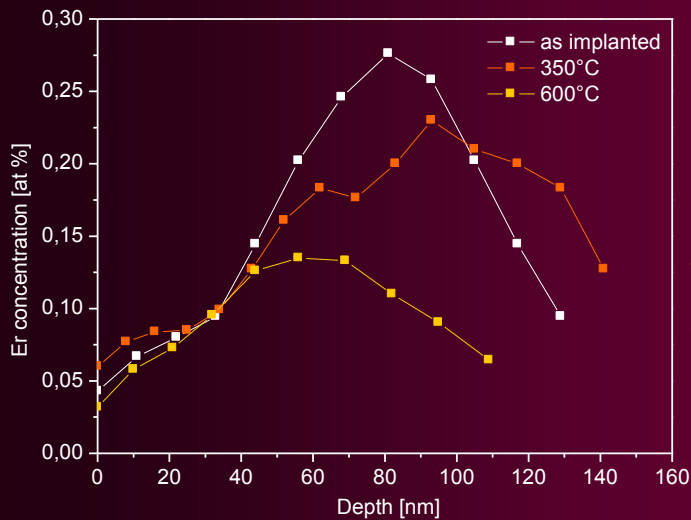


ION BEAMS PROVIDED BY SMALL ACCELERATOR

MALINSKÝ P., MACKOVÁ A., BOČAN J., ŠVEC OVÁ B., NEKVINDOVÁ P., Au implantation into various types of silicate glasses, Nuclear Instruments & Methods in Physics Research Section B. 267 (2009) 1575-1578

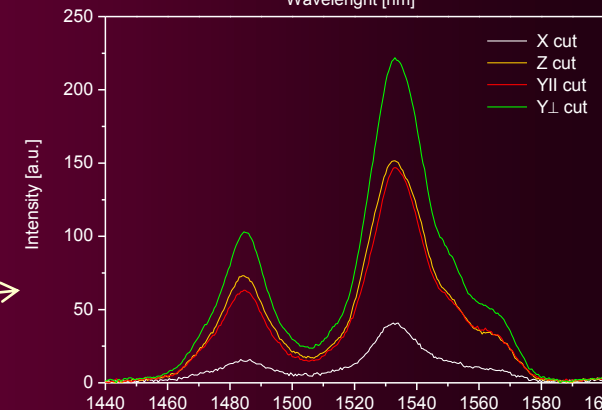
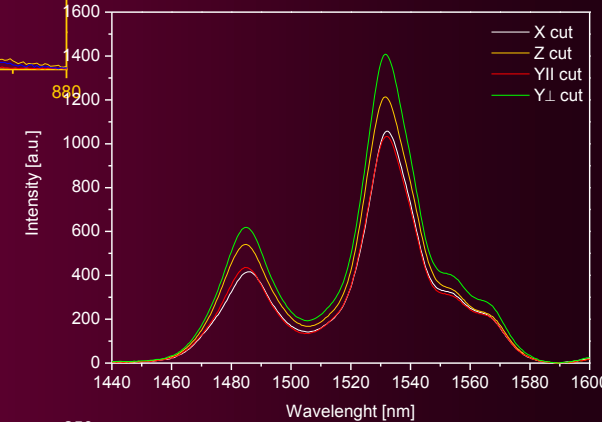
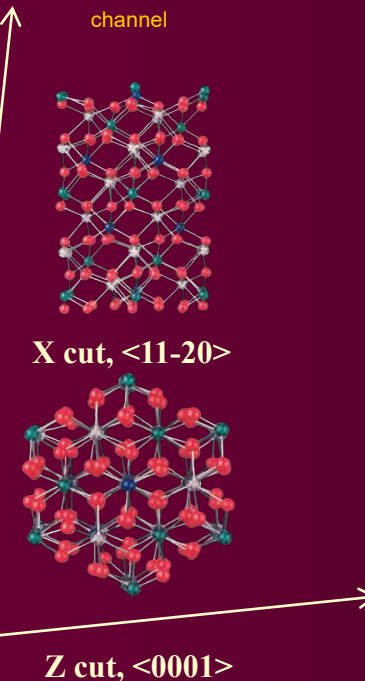
B. SVECOVA, P. NEKVINDOVA, A. MACKOVA, P. MALINSKY, A. KOLITSCH, V. MACHOVIC, S. STARA, M. MIKA, J. SPIRKOVA, Study of Cu⁺, Ag⁺ and Au⁺ ion implantation into silicate glasses, Journal of Non-Crystalline Solids, Volume 356, (2010), Issue 44-49, P. 2468-2472.

LiNbO₃ IMPLANTATION – RBS CHANNELING ANALYSIS



<0001> LN, 330keV, Er⁺ 2,5 x10¹⁵ cm⁻²

- RBS dopant depth profiling in as – implanted and as-annealed samples. RBS channeling structural study of the crystal recovery in different crystallographic orientation after the annealing procedure.
- The mechanism of recovery of the damaged structure of LN during the post-implantation annealing. In the Y⊥ cuts the recovery of LN lattice as well as defects migration is slow.
- In such a case erbium ions seem to be more mobile and do not create clusters, which was proved by broadening the erbium concentration profiles (RBS) and by increasing luminescence intensity.



LiNbO₃ IMPLANTATION – RBS CHANNELING ANALYSIS

Axial angle scan along the main crystallographic axes $\langle 0001 \rangle$, $\langle 01-10 \rangle$ and $\langle 11-20 \rangle$.

Er dopant positioning in crystalline matrix of LiNbO₃

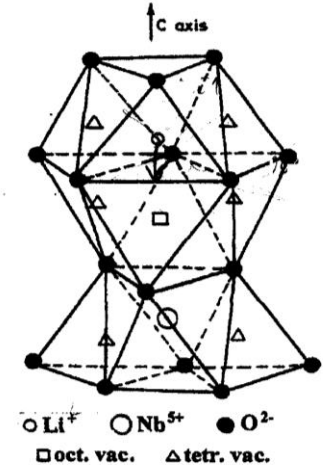
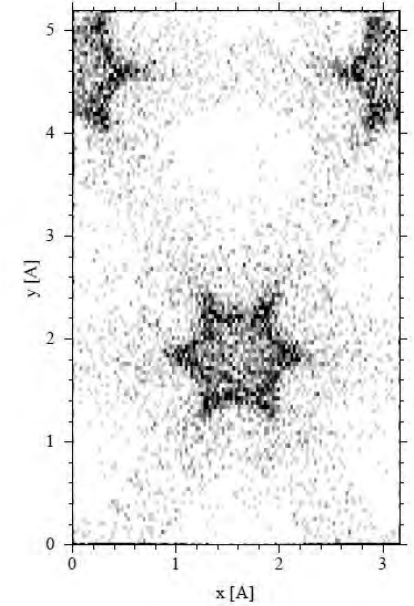
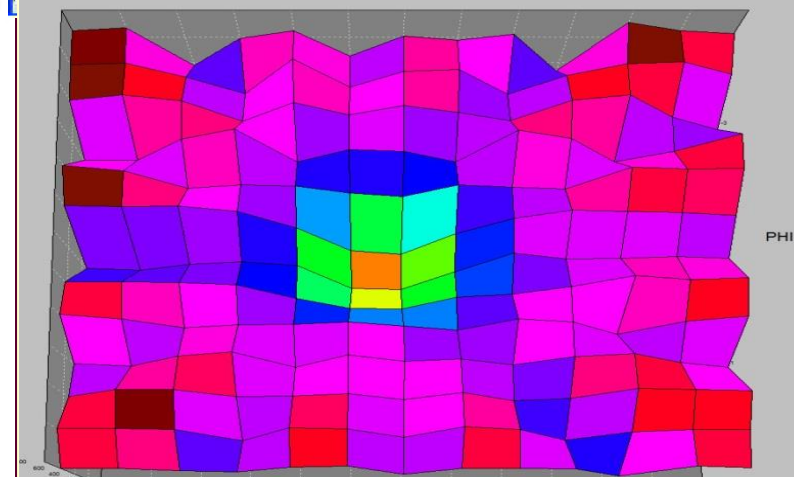
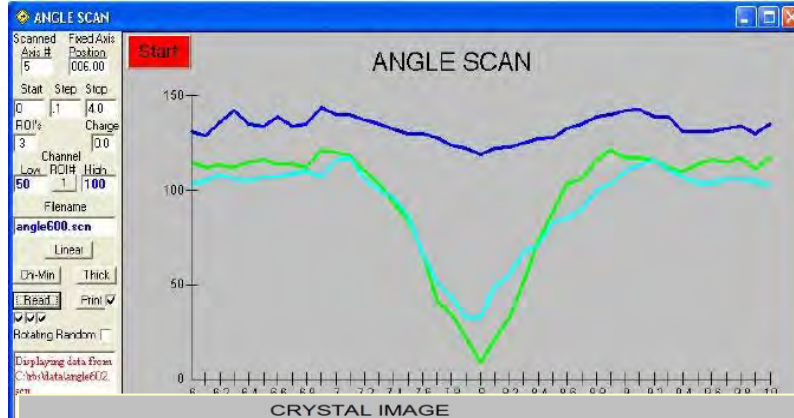
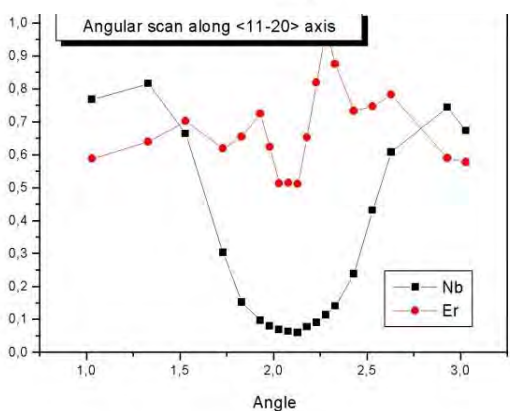
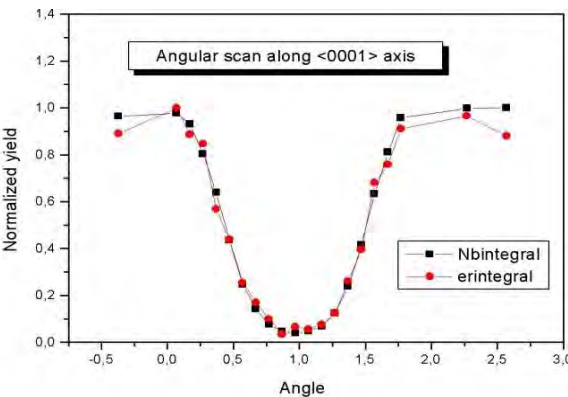
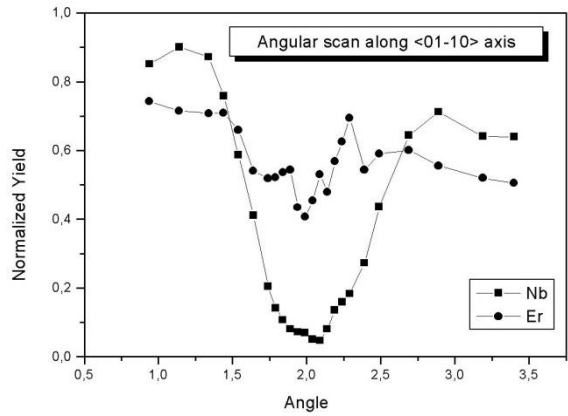


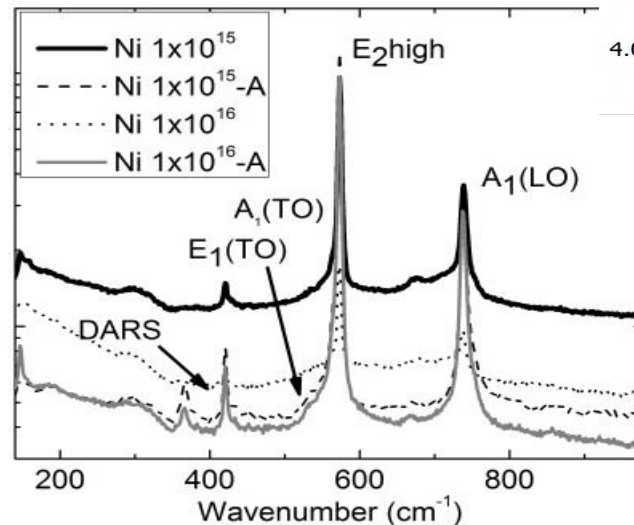
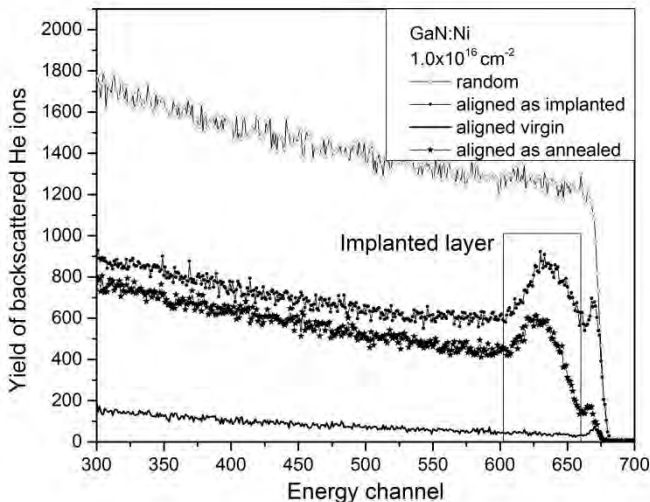
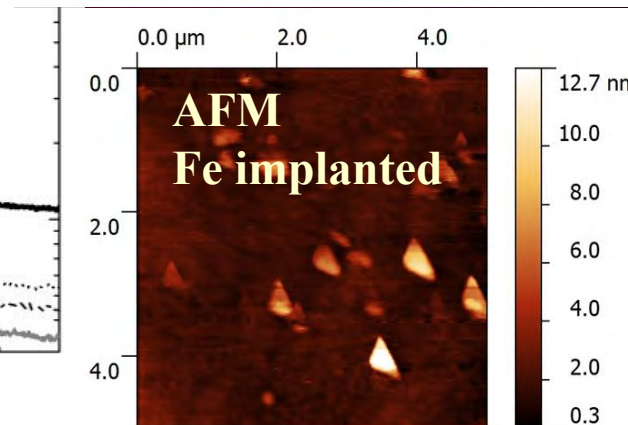
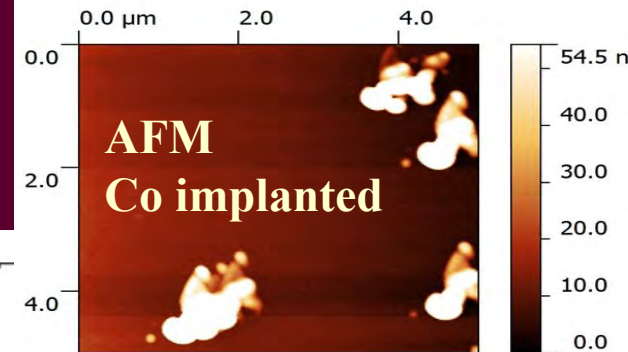
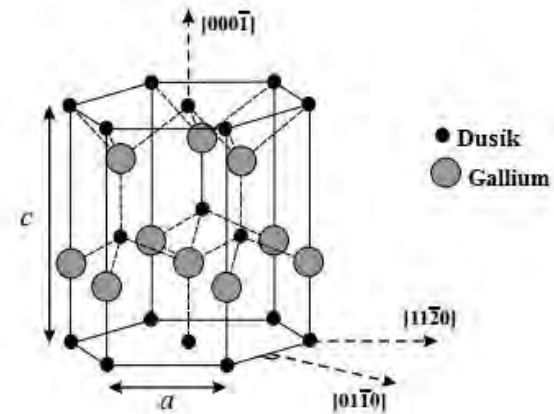
Fig. 2. Partial drawing of the unit cell of LiNbO₃ showing the four available sites for the RE³⁺ ions.



ION BEAMS PROVIDED BY SMALL ACCELERATOR

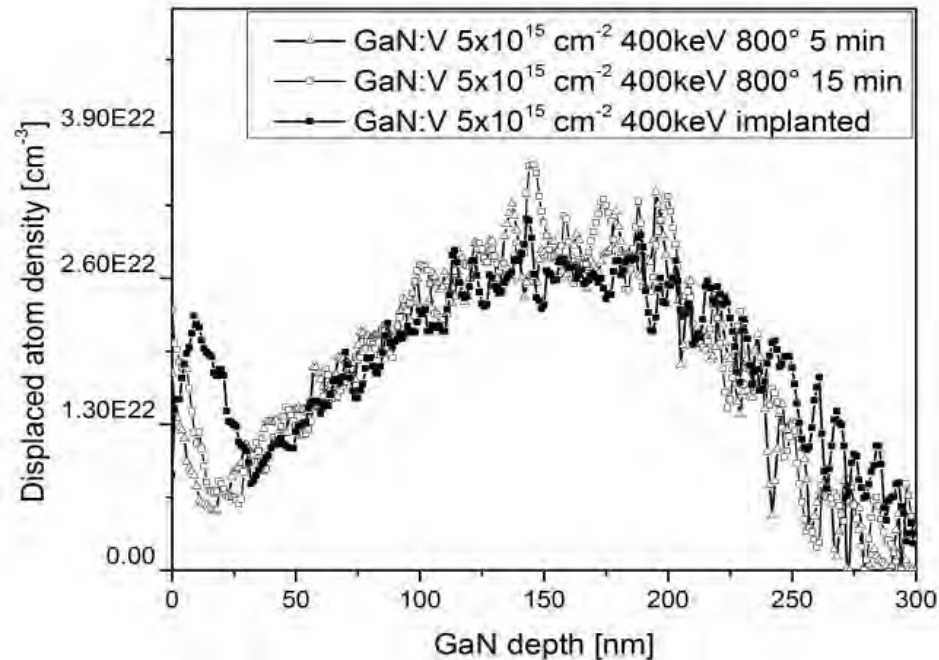
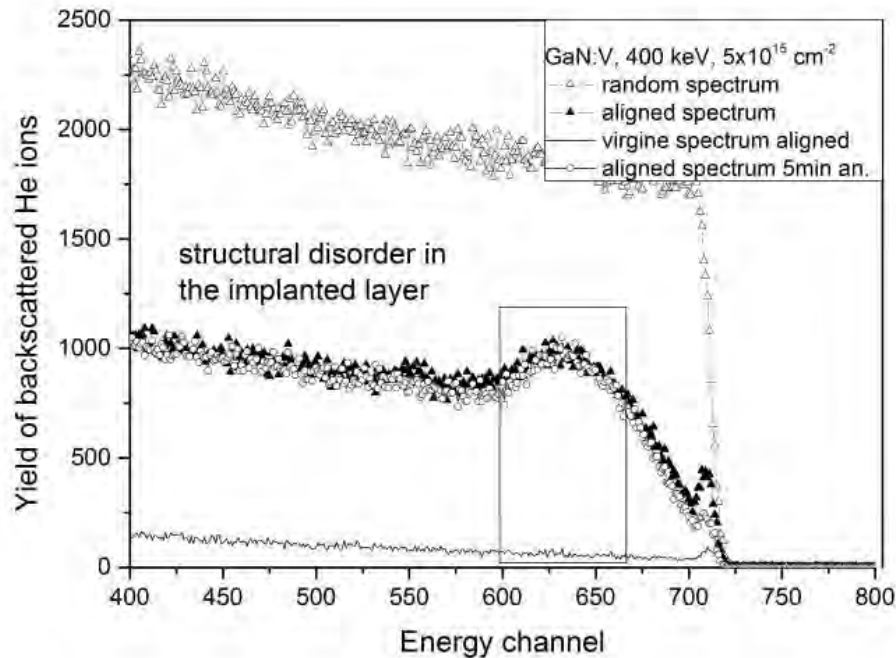
GaN TRANSITIONAL METAL ION IMPLANTATION

- Wide bandgap semiconductors such as GaN can be used for blue to ultraviolet (UV) light-emitting diodes, lasers, and detecting devices as well as high-frequency, high-temperature, and high-power electronic devices.
- Ion implantation is successfully used for this purposes, but in order to make the implanted ions optically and electrically active, the implantation damage-related defects must be annealed out without dissociation of host atoms.
- The structure after the annealing especially in the case of the $1 \times 10^{15} \text{cm}^{-2}$ implantation fluence is recovered significantly; some remaining disorder is presented in the implanted layer as shown by Raman spectroscopy. The surface morphology changes are influenced by the chemical properties of the implanted elements.



GaN TRANSITIONAL METAL ION IMPLANTATION

- A channeling RBS spectrum's yields (aligned spectrum), at a selected depth z , are increased by direct scattering of the channeled component from displacements and the scattering of the dechanneled component from lattice atoms. The usage of the known minimum yields depth profiles $c_D(z)$, which is deduced from the RBS aligned spectra enables us to extract by the iterative procedure the depth profiles of the displaced atoms by iterating channel by channel the aligned spectrum and converse it into the dislocated atoms density.
- A damage-buildup behavior is illustrated by the disorder depth profiles containing the surface peak caused by the surface disintegration under the high fluence implantation and the peak ascribed to the disorder distributed in the implanted layer.

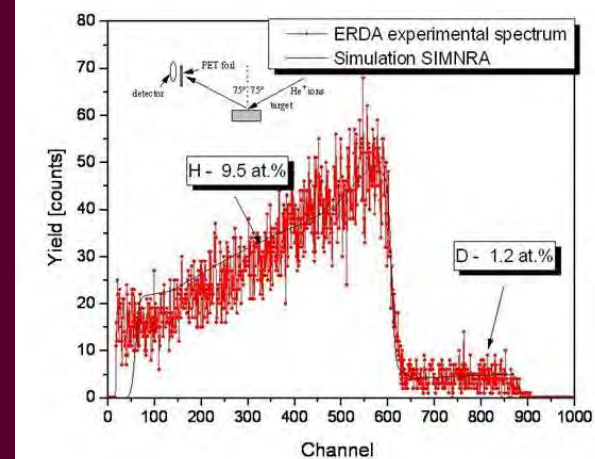
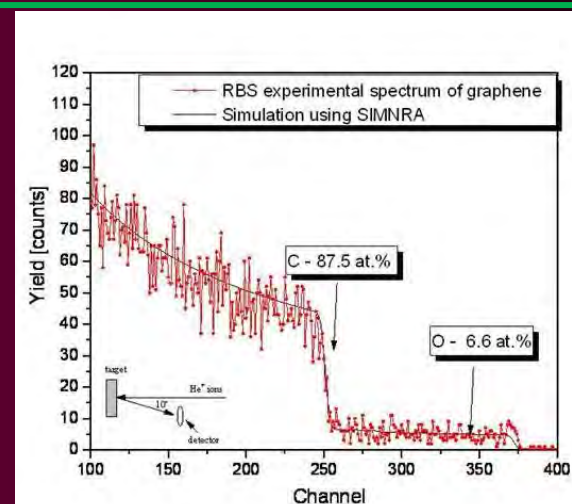
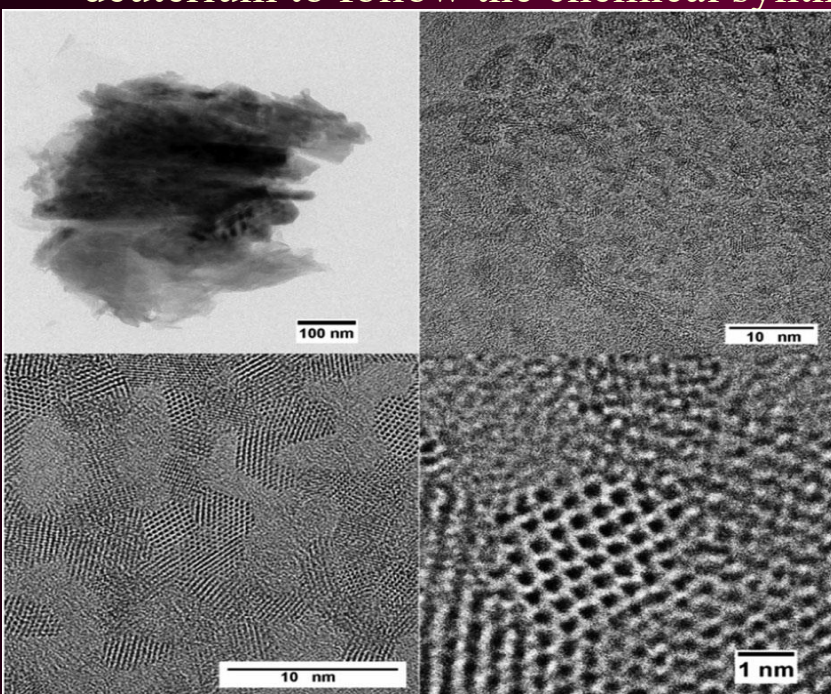


The structural and optical properties of metal ion-implanted GaN, Macková, Anna - Malinský, Petr - Sofer, Z. - Šimek, P. - Sedmidubský, D. - Veselý, M. - Bottger, R. Nuclear Instruments & Methods in Physics Research B 371 (2016) 254-257.

GRAPHENE BASED STRUCTURES CHARACTERIZED BY RBS and ERDA

Graphene, a two-dimensional (2D) sheet of carbon atoms arranged in a honeycomb lattice, attracted recently a huge scientific interest, due to its outstanding transport properties, chemical and mechanical stability and to the scalability of graphene devices to nanodimensions.

- Chemical synthesis of graphene relies on the usage of various chemical reagents.
- We demonstrated that these chemical treatments significantly contaminate graphene with heteroatoms/metals, depending on the procedures followed. Graphene was intentionally doped by deuterium to follow the chemical synthesis.



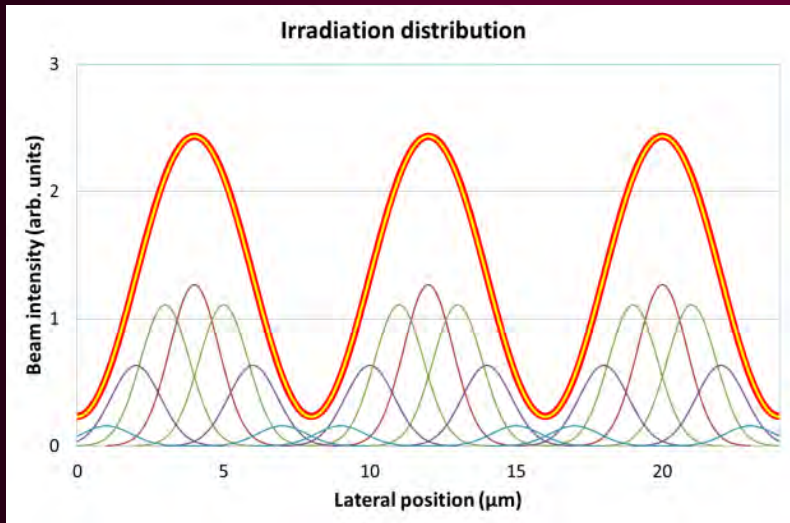
Jankovský, O. Šimek, P. Nováček, M. - Luxa, J. - Sedmidubský, D. - Pumera, M. - Macková, Anna - Mikšová, Romana - Sofer, Z. ,*RSC Advances*. Roč. 5, č. 24 (2015), s. 18733-18739.

Sofer, Z. - Jankovský, O. - Libánská, A. - Šimek, P. - Nováček, M. - Sedmidubský, D. - Macková, Anna - Mikšová, Romana - Pumera, M. ,*Nanoscale*. 7, 23 (2015), s. 10535-10543..

MICROBEAM APPLICATION ON ION BEM WRITING

Production of diffractive optical elements by modulating the refractive index of the material well below its surface by use of high energy ion implantation.

- to imitate interferometrically produced optical gratings by producing quasi-sinusoidal refractive index profiles making by modulating irradiation fluence across the grating lines, utilizing that the intensity distribution of the ion microbeam is close to Gaussian
- transmission phase optical gratings with grating constants ranging from 2 μm to 15 μm were designed and fabricated in Pyrex glass by 2 MeV H^+ and 6 MeV C^{3+} microbeam irradiation.



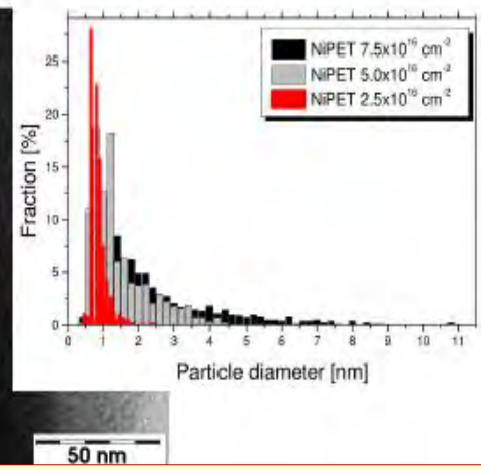
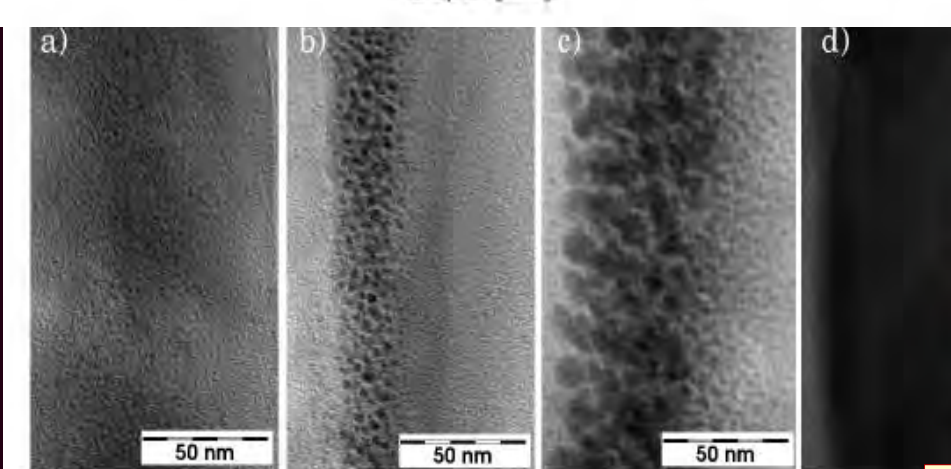
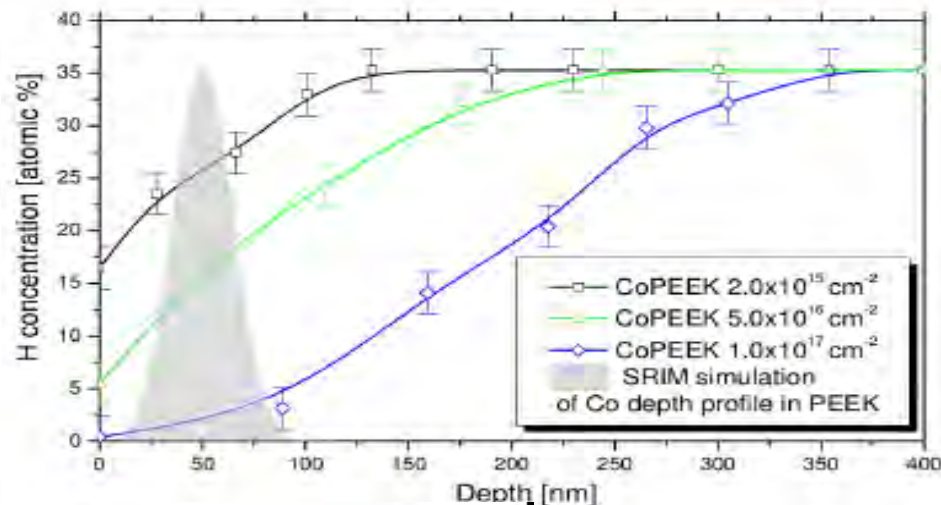
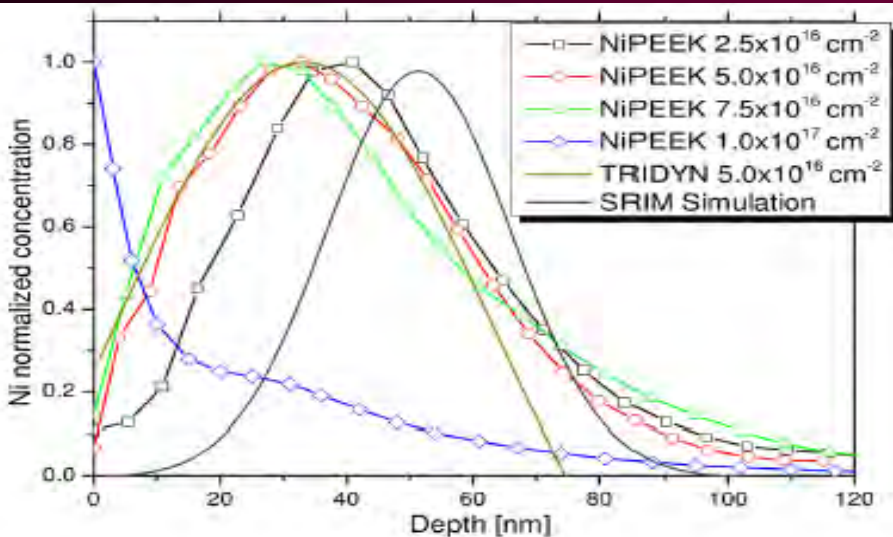
Banyasz, I.; Rajta, I.; Nagy, G. U. L.; Zolnai, Z.; Havránek, V. et al., Nuclear Instruments & Methods in Physics Research 331 (2014) 157-162

Banyasz, I.; Rajta, I.; Nagy, G. U. L.; Zolnai, Z.; Havránek, V. et al; Proceedings of SPIE, 8988 (2014) 898814.

POLYMER IMPLANTATION – RBS, ERDA

Metal/polymer nano-structured materials with shallow metal depth profiles are of the high importance for plastic electronics. Polyimide (PI), polyetheretherketone (PEEK), and polyethyleneterephthalate (PET) foils were implanted with 80 keV Co^+ ions at room temperature to the fluencies from $0,2 \times 10^{16} \text{ cm}^{-2}$ - $1,0 \times 10^{17} \text{ cm}^{-2}$. Oxygen and hydrogen depletion was examined using RBS and ERDA techniques.

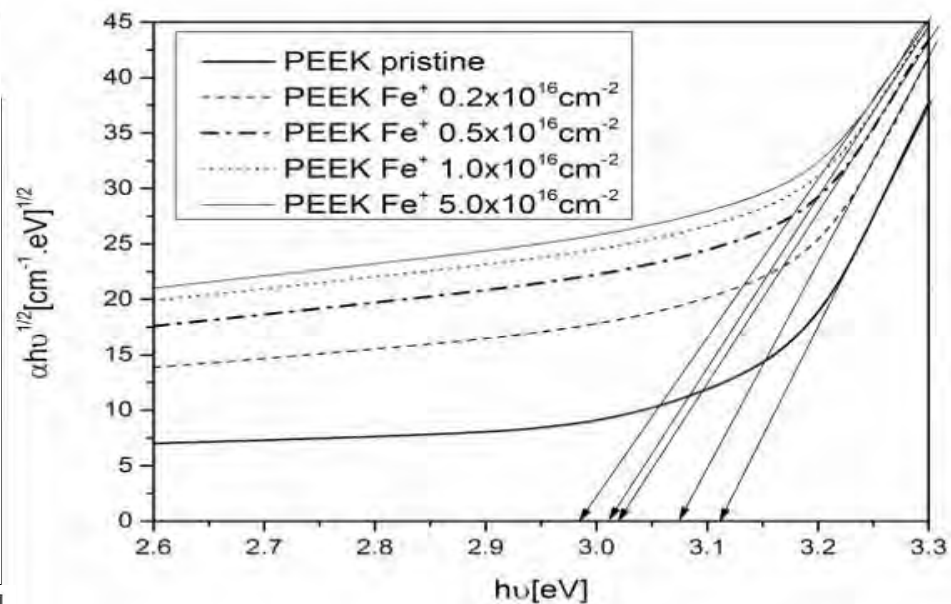
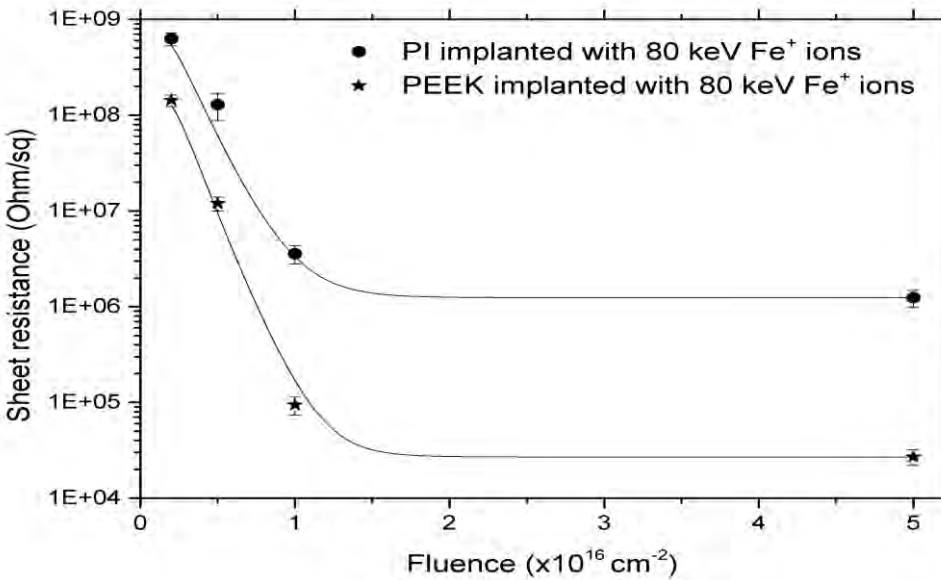
The most dramatic changes in electrical resistivity with the increasing ion implantation fluence were observed in PEEK. The Co particles with the largest diameter were observed in PET samples.



A. Mackova, et al, Nucl. Instrum. Meth. B 331 (2014), p.176–181
 A. Mackova, P. Malinsky, R. Miksova, H. Pupikova, R. I. Khaibullin, P. Slepicka, A. Gombitova, L. Kovacik, V. Svorecik, Nucl. Instrum. Meth. B 325 (2014), p.89–96

ELECTRICAL AND OPTICAL PROPERTIES OF IMPLANTED POLYMERS

Surface electrical resistivity of the metal ion implanted polymers as a decreasing function of the ion implantation fluence in connection to electronic and structural changes of irradiated polymers. a UV VIS spectroscopy indicates the absorption edge shift and saturation effect with ion implantation fluence.



Polymer	Fluence of Fe ion beam	Band gap (eV) Indirect
PEEK	Pristine	3.11
	$0.2 \times 10^{16} \text{ ion/cm}^2$	3.07
	$0.5 \times 10^{16} \text{ ion/cm}^2$	3.02
	$1.0 \times 10^{16} \text{ ion/cm}^2$	3.01
	$5.0 \times 10^{16} \text{ ion/cm}^2$	2.98
PI	Pristine	2.24
	$0.2 \times 10^{16} \text{ ion/cm}^2$	2.17
	$0.5 \times 10^{16} \text{ ion/cm}^2$	2.15
	$1.0 \times 10^{16} \text{ ion/cm}^2$	2.12
	$5.0 \times 10^{16} \text{ ion/cm}^2$	2.10
PET	Pristine	3.89
	$0.2 \times 10^{16} \text{ ion/cm}^2$	3.85
	$0.5 \times 10^{16} \text{ ion/cm}^2$	3.84
	$1.0 \times 10^{16} \text{ ion/cm}^2$	3.82
	$5.0 \times 10^{16} \text{ ion/cm}^2$	3.77

Tauc expression $\alpha(\nu)h\nu = B(h\nu - E_g)^n$
 $\alpha(\nu)$ – absorption coefficient dependence on the electromagnetic radiation frequency ν , n chosen for direct or indirect transitions

P. Malinsky, A. Mackova et al, Nucl. Inst. and Meth. B, Vol. 272 (2012) p.396-399

ENERGY STOPPING OF ENERGETIC IONS

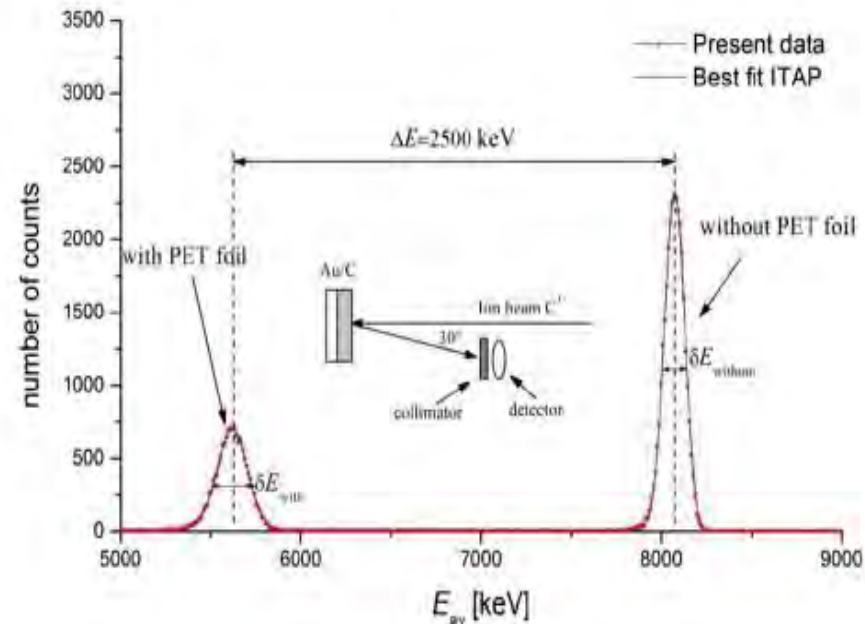
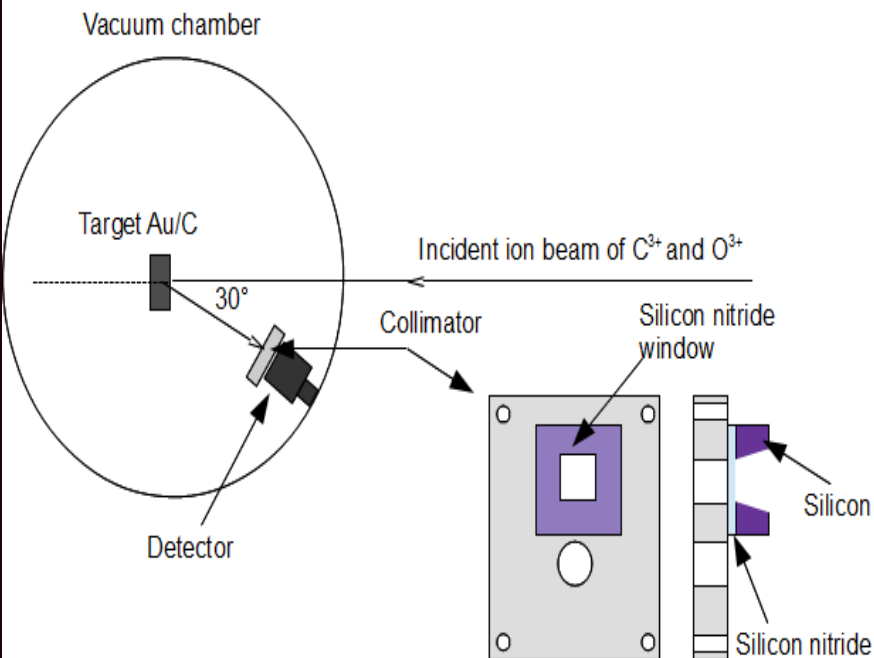
ΔE is the energy loss in the foil and Δt is the thickness of the foil

$$S = \frac{\Delta E}{\Delta t}$$

E_1 is the energy of the ions backscattered from the Nb surface layer. The energy of backscattered ions is deduced from the formula $E_1 = K.E$
 E is the incident ion energy



- The stopping power and energy straggling of energetic ions in matter is important to many applications dependent on the transport of ions in matter such as:
- ion beam analysis techniques, and in consequences in the application of metal composites in microelectronics optoelectronics prepared by ion implantation
- the dosimetry of ions and radiology or radiation safety due to similarity of polymers to human tissue.



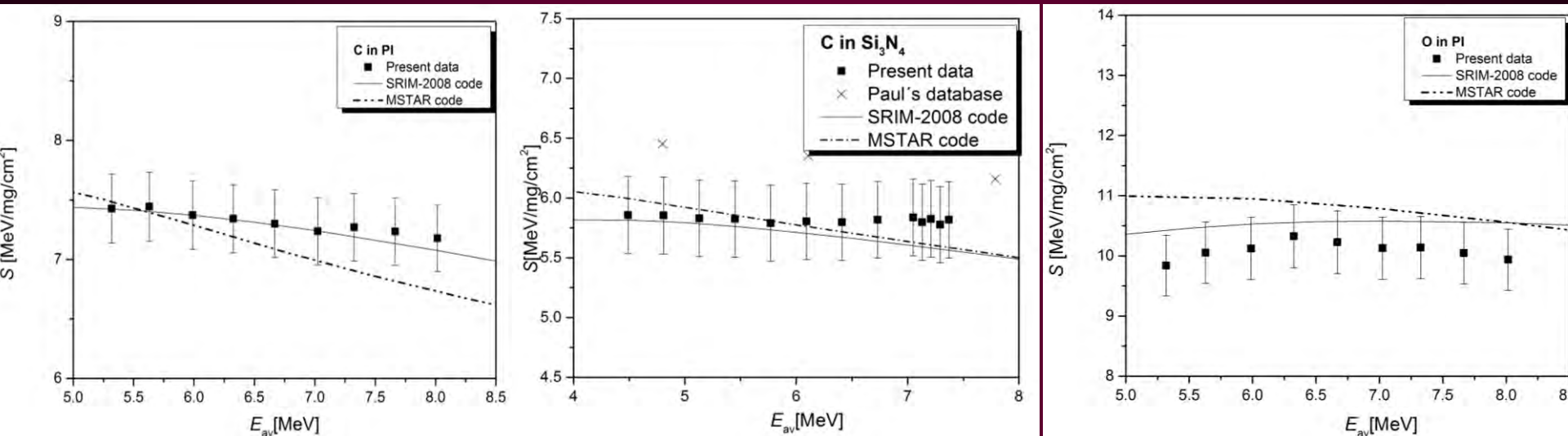
ION BEAMS PROVIDED BY SMALL ACCELERATOR

ENERGY STOPPING OF ENERGETIC IONS

The stopping powers of Li, Co and O ions in the mean energy range of 3 - 10 MeV for PC, PP, PI etc. compared to the theoretical predictions made by the SRIM and MSTAR codes.

The measured stopping powers agree within the quoted error with those calculated with SRIM code with implemented CAB model for both ions species.

The significant deviation between the measured stopping powers of the ions in the compounds and the MSTAR-code calculation based on Bragg's rule is caused by the differences in chemical and electronic structure of the investigated polymers.



R. Mikšová, A. Macková, P. Malinský, P. Slepíčka, V. Švorčík, A study of the degradation of polymers irradiated by Cn⁺ and On⁺ 9.6 MeV heavy ions, *Polymer Degradation and Stability*, Volume 122, (2015) 110-121.

R. Mikšova, A. Mackova, P. Malinsky, V. Hnatowicz, P. Slepicka *Nuclear Instruments and Methods in Physics Research B* 331 (2014) 42–47

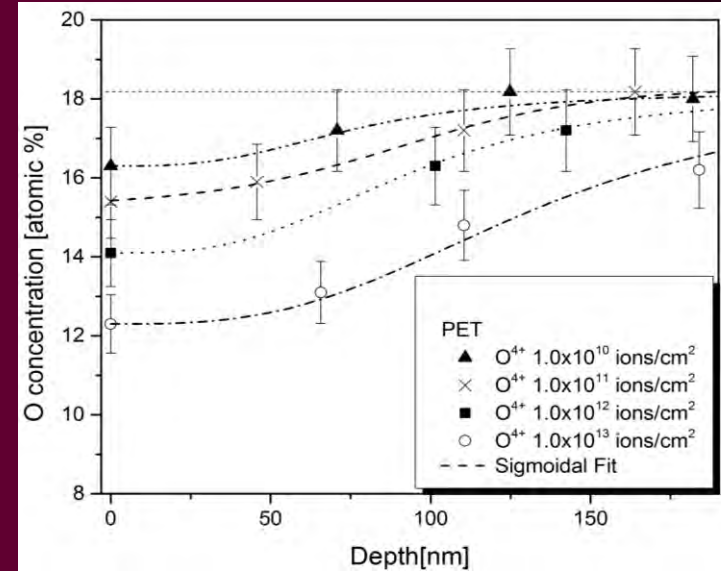
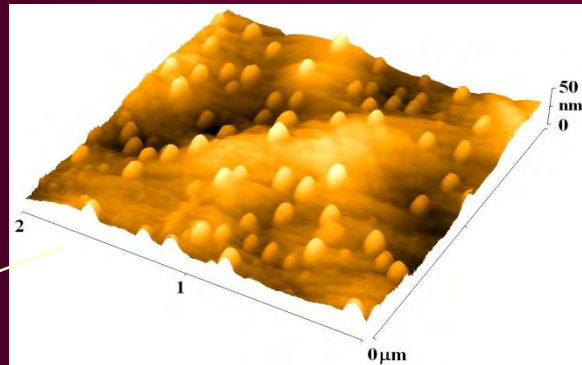
ENERGY STOPPING OF ENERGETIC IONS

- Ω_i and Ω_f are the variances of RBS signals for direct and slowed down beams, respectively. S_f and S_i are the ion stopping powers at the entrance and exit of the polymer foil, respectively.

- the theoretical predictions of the Bohr theory Ω_B were done by SIMNRA 6.06.

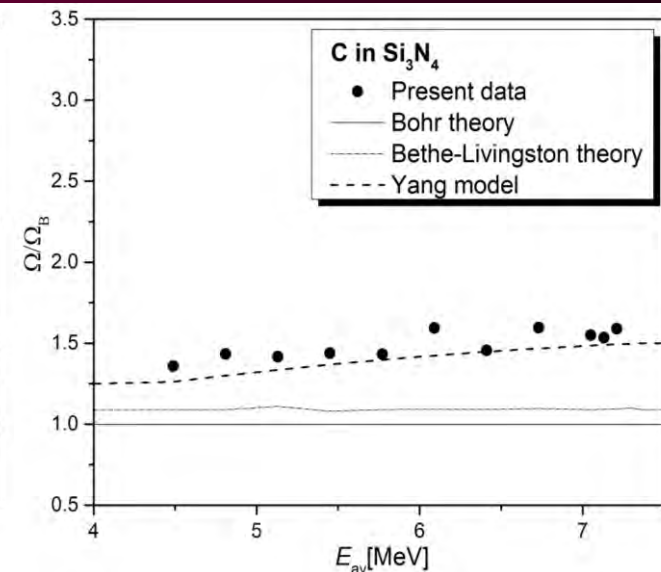
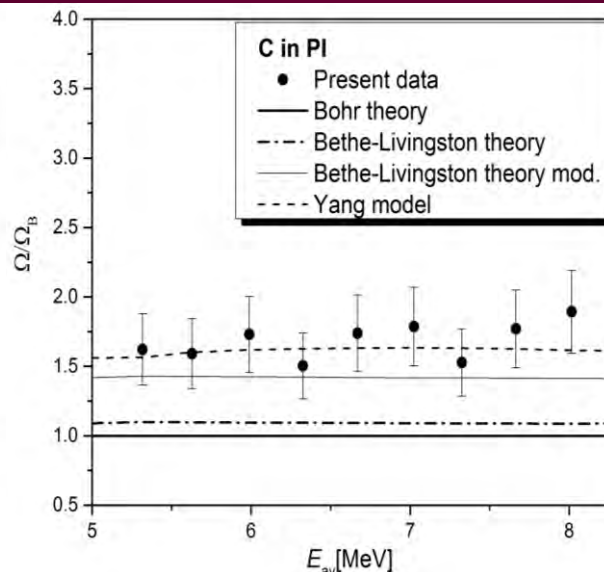
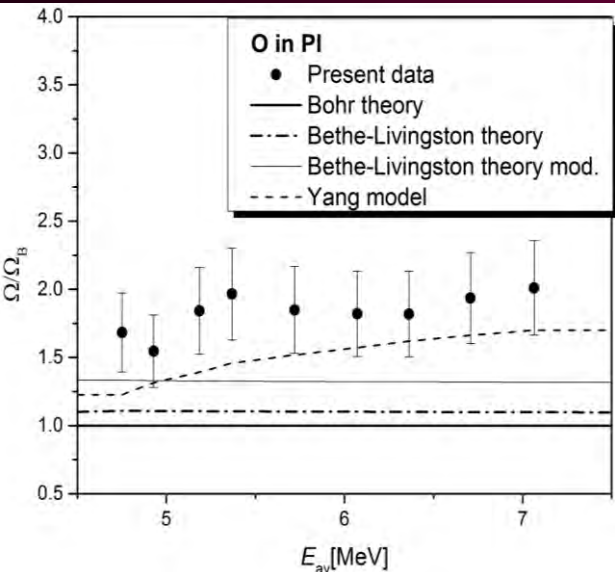
RBS light element depth profiling

$$\Omega^2 = \left(\frac{S_f}{S_i} \right)^2 \Omega_i^2$$



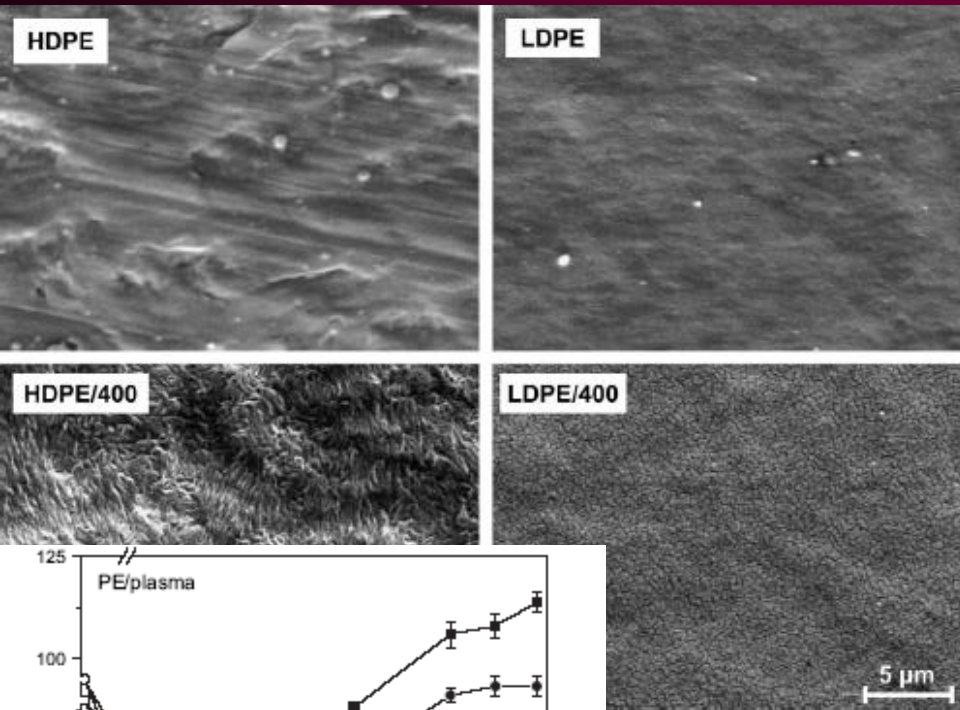
$$\Omega^2 = \Omega_{exp}^2 - \delta^2 \cdot \Delta E^2$$

The reduced energy straggling Ω/Ω_B

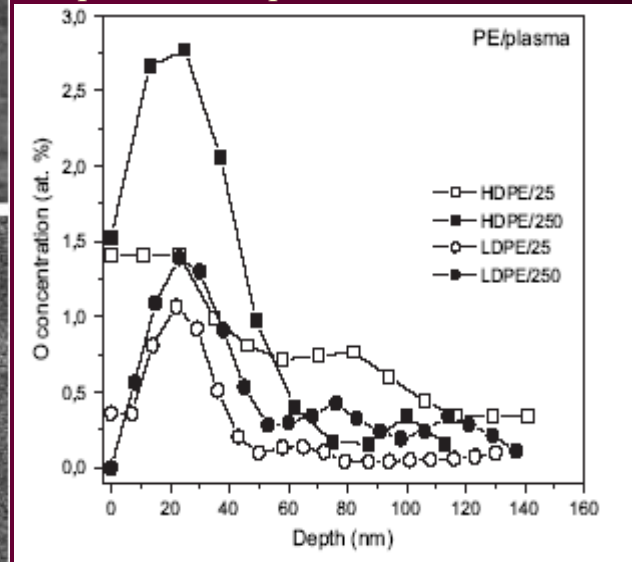


ION BEAMS FOR BIO-MATERIALS

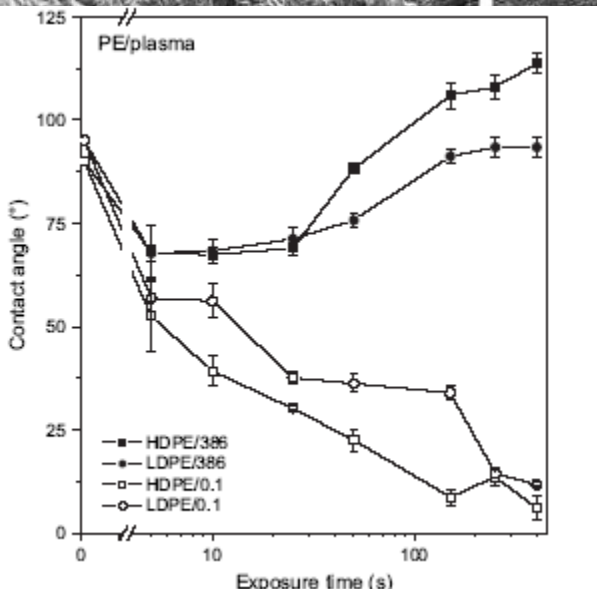
The irradiation of non-polar polyolefins (PE, PP, PS and fluoropolymers) leads to creation of polar groups on the polymer surface and in this way it enhances printability, wettability, adhesion with inorganic materials (e.g. metals) or with biologically active components. One of the possible modification techniques is the



The SEM images of PE foils before (HDPE and LDPE) and after 400 s (HDPE/400, LDPE/400) modification in Ar plasma with power 1.7 W



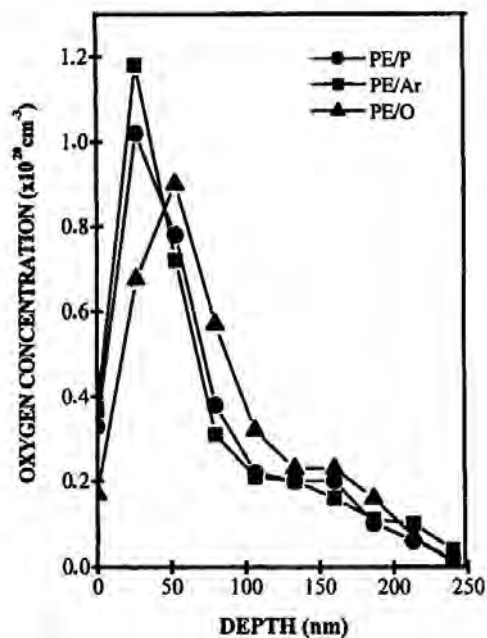
Concentration depth profile of oxygen incorporated in HDPE and LDPE. The profiles were determined by RBS technique.



The dependence of the contact angle on the plasma exposure time for LDPE and HDPE measured 0.1 h (0.1) and 386 h (386) after the exposure to plasma discharge of 1.7 W power

Nanostructuring of polymethylpentene by plasma and heat treatment for improved biocompatibility, P. Slepíčka, S. Trostová, N. Slepíčková Kasálková, Z. Kolská, P. Malinský, A. Macková, L. Bačáková, V. Švorčík, POLYMER DEGRADATION AND STABILITY Volume: 97 Issue: 7 Pages: 1075-1082, 2012

ION BEAMS FOR BIO-MATERIALS

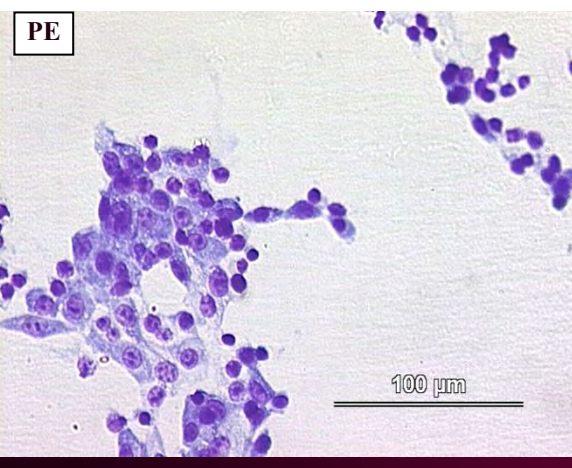
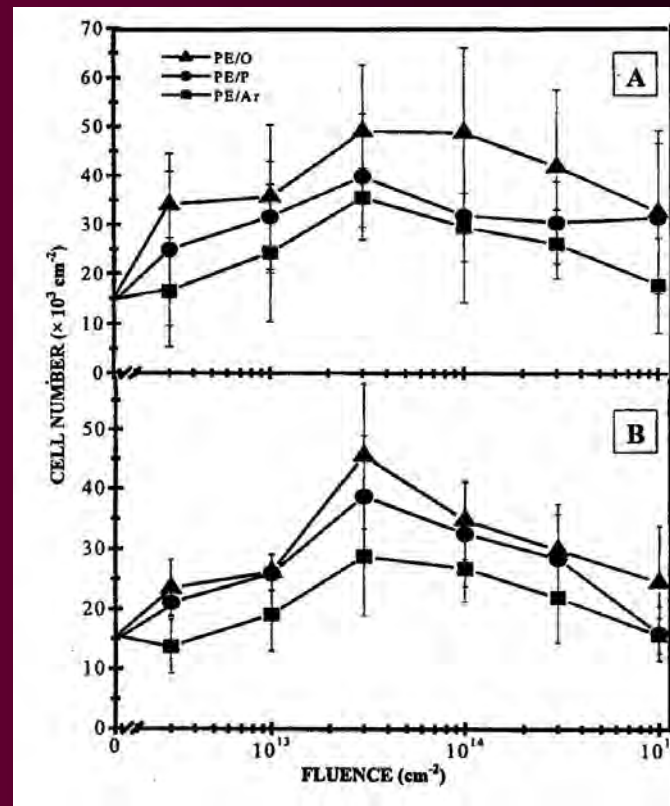


The investigation of ion beam modified polymers as materials with better bio-functionality and bio-compatibility and potential application in medicine.

Oxidation of the polymer surface upon ion irradiation increases its wettability and surface polarity.

Bio-compatibility tests

- surface wettability and polarity
- cell adhesion on the surface
- cell proliferation and cultivation



For all ion species the maximum adhesion was observed for the ion fluence of $3 \times 10^{13} \text{ cm}^{-2}$. It can be concluded that the optimum surface polarity exists for which the adhesion achieves a maximum.

Cytocompatibility of Ar⁺ plasma treated and Au nanoparticle-grafted PE, V. Švorcik, N. Kasalkova, P. Slepicka, K. Zaruba, V. Kral, L. Bacakova, A. Mackova, M. Parizek et al., Nuclear Instruments and Methods in Physics Research B 267 (2009) 1904–1910

CONCLUSIONS

Ion beam analysis gives us opportunity to get a complex information about the investigated structures and materials.

These analytical methods are irreplaceable in material research.

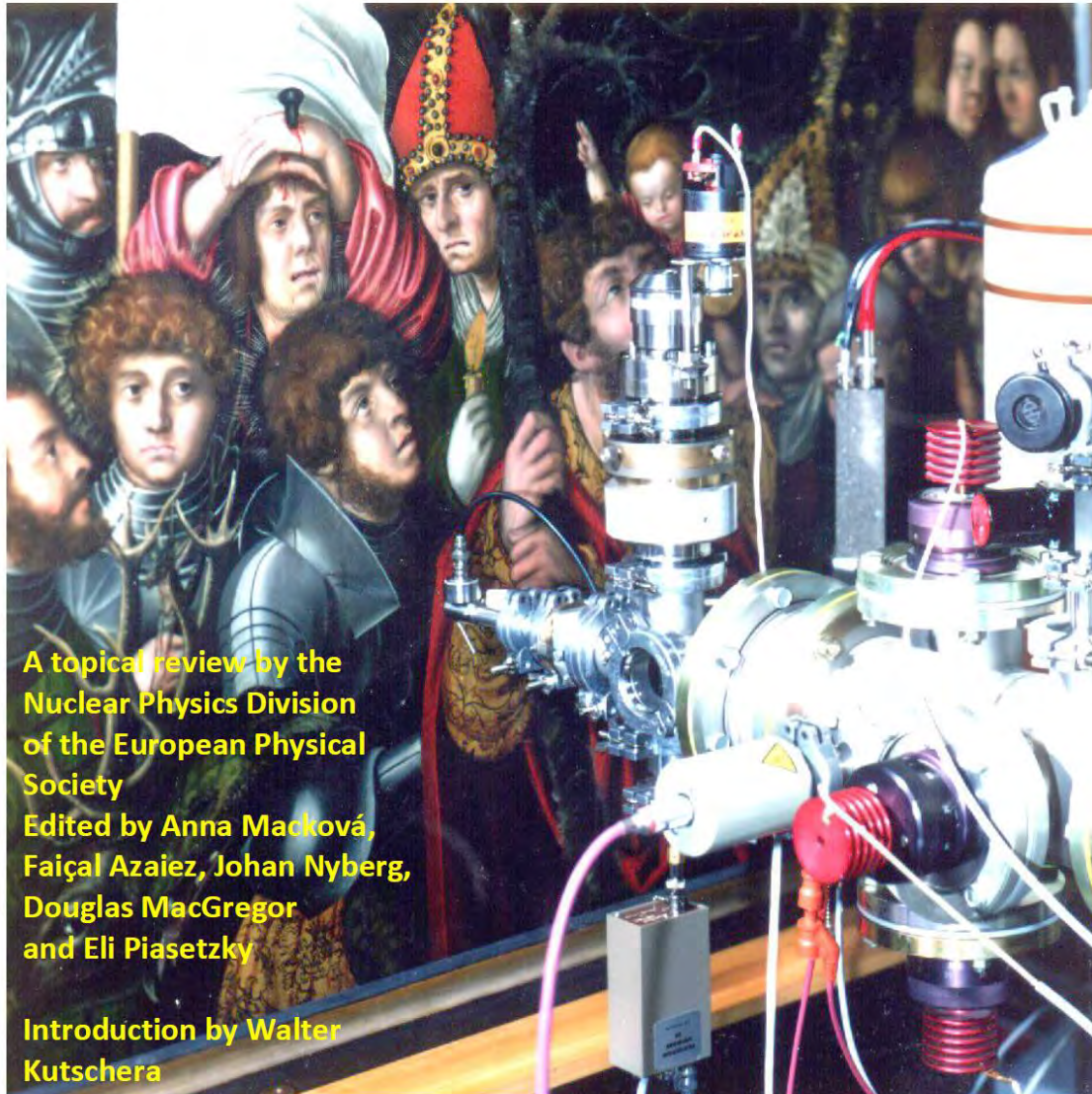
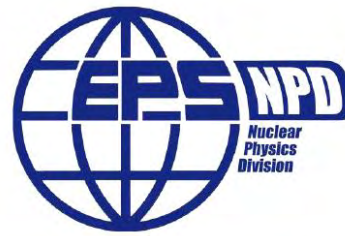
Ion beams are powerful tool for material modification, new structure preparation and study of basic processes taking place in solid state after the irradiation by energetic ions.

Acknowledgements

The research was realized at the CANAM (Center of Accelerators and Nuclear Analytical Methods) infrastructure and has been supported by project P108/12/G108.

This work has been supported by the European Community as an Integrating Activity SPIRIT under EC contract no. 227012.

NUCLEAR PHYSICS FOR CULTURAL HERITAGE



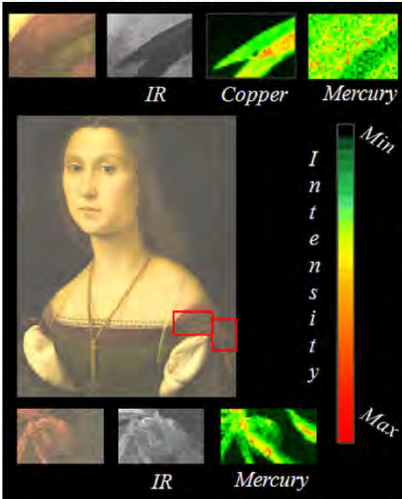
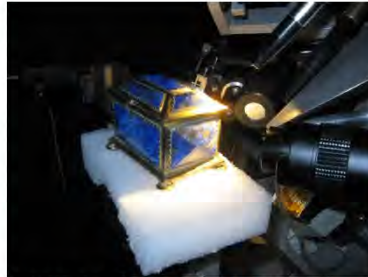
A topical review by the
Nuclear Physics Division
of the European Physical
Society

Edited by Anna Macková,
Faïçal Azaiez, Johan Nyberg,
Douglas MacGregor
and Eli Piassetzky

Introduction by Walter
Kutschera

Cultural heritage studies

- The ion microbeam set-up has proven to be versatile and allows many analytical techniques to be in combination. The ion beam is focused onto a spot as small as a few hundred nanometers in diameter. By scanning the beam over the sample surface a 2D distribution of elements can be determined. Varying the ion beam energy may even allow a 3D distribution to be obtained. The results are elemental maps of the investigated artefact. The determination of trace elements often allows information to be deduced regarding the origin of the artefact or its manufacturing process.

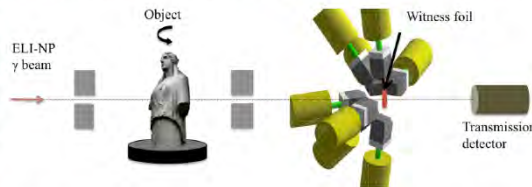


- Neutron beams offer a wide range of possibilities to explore the compositional or structural features of the samples. The low energy and relatively low intensity of guided neutron beams ensure no long-term damage is done to the objects studied and any induced radioactivity

generally decays within a few days. Neutron beam tomography is used to map the internal structure and morphology of historical artefacts and teaches us about ancient production technologies.

- Radiocarbon dating provided by AMS has proved to be one of the most useful dating tools for archaeological, environmental and geological studies which all benefit from the ability to date organic materials.
- X-ray fluorescence is a valuable technique used in the elemental identification of cultural heritage objects because it is non-invasive, non-destructive, and highly sensitive. It is a quantitative technique which can, in many cases, be used directly on the surface of the objects to provide information about the chemical composition of inks and paint pigments.

- The European initiative for Extreme Light Infrastructure laboratories in Romania (ELI-NP), will shortly provide tunable energy γ -rays from inverse Compton scattering of laser light on a high-energy electron beam. This will allow Nuclear Resonance Fluorescence studies of isotope-specific trace element distributions to be performed with unprecedented sensitivity. It is planned to use this powerful tool for cultural heritage object studies.



- Preservation often requires high intensities of irradiation. One of the main applications is the sterilisation of an object by γ -rays, a method widely used for medical equipment. The purpose is to kill any bacteria, fungi, or woodworms which would otherwise destroy the object over a period of time.
- The topical review paper is extensively illustrated with important discoveries and examples from archaeology, pre-history, history, geography, culture, religion and curation, which underline the breadth and importance of this field.

European facilities using nuclear techniques to study cultural heritage

The map below shows the spread of permanent laboratories and centres with facilities used for nuclear physics studies of Cultural Heritage objects across Europe.

- Ion Beam Analysis Facilities in Europe
- European Neutron Sources
- European Accelerator Mass Spectrometry Facilities
- Other European Centres, Facilities and Laboratories



- The large number of groups and laboratories contributing to the study and preservation of cultural heritage across Europe indicate the enormous effort and importance of this activity.

- For more detail the full paper can be downloaded from the EPS website: <http://xxx.xxx.xxx>